CANCER

Enhancing KDM5A and TLR activity improves the response to immune checkpoint blockade

Liangliang Wang[1]*, Yan Gao[1,2]*, Gao Zhang[3]*, Dan Li[1]*, Zhenda Wang[1], Jie Zhang[4], Leandro C. Hermida[5,6], Lei He[1], Zhisong Wang[1], Jingwen Si[1], Shuang Geng[7], Rizi Ai[8], Fei Ning[9], Chaoran Cheng[4], Haiteng Deng[10], Dimiter S. Dimitrov[11], Yan Sun[12], Yanyi Huang[7], Dong Wang[13], Xiaoyu Hu[9†], Zhi Wei[4†], Wei Wang[8†], Xuebin Liao[1†]

Immune checkpoint blockade (ICB) therapies are now established as first-line treatments for multiple cancers, but many patients do not derive long-term benefit from ICB. Here, we report that increased amounts of histone 3 lysine 4 demethylase KDM5A in tumors markedly improved response to the treatment with the programmed cell death protein 1 (PD-1) antibody in mouse cancer models. In a screen for molecules that increased KDM5A abundance, we identified one (D18) that increased the efficacy of various ICB agents in three murine cancer models when used as a combination therapy. D18 potentiated ICB efficacy through two orthogonal mechanisms: (i) increasing KDM5A abundance, which suppressed expression of the gene *PTEN* (encoding phosphatase and tensin homolog) and increased programmed cell death ligand 1 abundance through a pathway involving PI3K-AKT-S6K1, and (ii) activating Toll-like receptors 7 and 8 (TLR7/8) signaling pathways. Combination treatment increased T cell activation and expansion, $CD103^+$ tumor-infiltrating dendritic cells, and tumor-associated M1 macrophages, ultimately enhancing the overall recruitment of activated $CD8^+$ T cells to tumors. In patients with melanoma, a high *KDM5A* gene signature correlated with *KDM5A* expression and could potentially serve as a marker of response to anti–PD-1 immunotherapy. Furthermore, our results indicated that bifunctional agents that enhance both KDM5A and TLR activity warrant investigation as combination therapies with ICB agents.

INTRODUCTION

The treatment of various cancers has been revolutionized by the development of effective immunotherapies that are now established as powerful clinical tools (*1*). Many of these promising immunotherapeutic strategies, which lead to strong antitumor responses and sometimes even long-term remissions, are based on the blockade of activation of immune inhibitory receptors found on activated T cells or other immune cells. Such immunotherapeutic targets currently include cytotoxic T lymphocyte–associated protein 4, programmed cell death protein 1 (PD-1), and programmed cell death ligand 1 (PD-L1) (*2*), among others. Unfortunately, only a minority of patients respond to any particular immune checkpoint blockade (ICB) agent (*1*). Therefore, it is anticipated that combination immunotherapies targeting nonredundant immune pathways will be required to improve upon both the efficacy and response rates of ICB therapies (*3*, *4*). Efforts to identify combination agents mostly focused on immune targets.

Tumors often exhibit extensive epigenetic reprogramming, for example, with tumor cell genomes displaying histone 3 lysine 4 trimethylation (H3K4me3) marks that induce gene transcription (*5*). The H3K4 demethylase KDM5A (also referred to RBP2 or JARID1A) acts on tri- and dilysine 4 of histone H3 (H3K4me3/2) but does not demethylate monomethylated H3K4 (*6*, *7*). *KDM5A* is a potential oncogene in various cancers (*8*). Because KDM5A promotes drug resistance in certain cancer cells (*9*) and is associated with tumorigenesis and metastasis, this protein represents a potential therapeutic target for inhibition (*7*).

Several studies have reported that histone (de-)methylases are involved in overcoming tumor resistance to PD-1/PD-L1 blockade (*10*–*12*). For example, inhibiting the lysine-specific histone demethylase 1A (also referred to KDM1A) in conjunction with administering anti–PD-1 antibody triggered antitumor immunity and reduced tumor growth in a B16 melanoma model (*10*). Despite the importance of KDM5A in both normal physiology and disease, it is unknown whether inhibiting or enhancing KDM5A activity will improve the response to ICB. Motivated by this emerging understanding of the potential impact of altered demethylation activity on immunotherapy outcomes, we explored publicly available RNA sequencing (RNA-seq) data from two large-scale cancer genomics resources and published ICB studies. Our analysis suggested that a *KDM5A* gene signature might be a potential marker for predicting patients that would respond to anti–PD-1 therapy.

To explore the relationship between KDM5A and anti–PD-1 responses, we used mouse models of colon cancer and melanoma.

[1]School of Pharmaceutical Sciences, Key Laboratory of Bioorganic Phosphorus Chemistry and Chemical Biology (Ministry of Education), Beijing Advanced Innovation Center for Human Brain Protection, Tsinghua University, Beijing 100084, China. [2]Beijing Obstetrics and Gynecology Hospital, Capital Medical University, Beijing 100006, China. [3]Department of Neurosurgery and The Preston Robert Tisch Brain Tumor Center, Duke University Medical Center, Durham, NC 27710, USA. [4]Department of Computer Science, College of Computing Sciences, New Jersey Institute of Technology, Newark, NJ 07102, USA. [5]Center for Cancer Research, National Cancer Institute, National Institutes of Health, Bethesda, MD 20892, USA. [6]Center for Bioinformatics and Computational Biology, Department of Computer Science, University of Maryland, College Park, MD 20742, USA. [7]Biomedical Pioneering Innovation Center (BIOPIC), Beijing Advanced Innovation Center for Genomics (ICG), College of Chemistry, Peking-Tsinghua Center for Life Sciences, Peking University, Beijing 100871, China. [8]Department of Chemistry and Biochemistry, 9500 Gilman Drive, UC San Diego, La Jolla, CA 92093, USA. [9]Institute of Immunology and School of Medicine, Tsinghua University, Beijing 100084, China. [10]MOE Key Laboratory of Bioinformatics, School of Life Sciences, Tsinghua University, Beijing 100084, China. [11]Department of Medicine, University of Pittsburgh, Pittsburgh, PA 15261, USA. [12]Lanzhou Institute of Husbandry and Pharmaceutical Science of CAAS, Lanzhou 730050, China. [13]School of Basic Medical Sciences, Chengdu University of Traditional Chinese Medicine, Chengdu 611137, China.
*These authors contributed equally to this work.
†Corresponding author. Email: xiaoyuhu@mail.tsinghua.edu.cn (X.H.); zhiwei04@gmail.com (Z. Wei); wei-wang@ucsd.edu (W.W.); liaoxuebin@mail.tsinghua.edu.cn (X.L.)

We showed that overexpression of KDM5A in tumor cells renders MC38 colon cancer and B16 melanoma more responsive to anti–PD-1 therapy and provided evidence that this effect of KDM5A occurred down-regulating *PTEN* expression, activating the PI3K (phosphatidylinositol 3-kinase)–AKT–S6K1 (S6 kinase 1) signaling cascade and increasing the abundance of PD-L1. Because high PD-L1 abundance in tumors leads to effective anti–PD-L1 immunotherapies (*13*), we screened for potential combination agents that increased the abundance of both KDM5A and PD-L1. We found that a potential drug candidate D18 both increases the abundance of KDM5A and PD-L1, as well as acts as Toll-like receptors 7 and 8 (TLR7/8) agonist. We also found that the combination of D18 with various ICB agents suppressed the growth rate of tumors in mice. The combination treatment increased T cell expansion, infiltration, tumor-infiltrating $CD103^+$ dendritic cells (DCs), and tumor-associated M1 macrophages, thereby increasing the overall recruitment of activated $CD8^+$ T cells into the tumor microenvironment (TME).

RESULTS

A *KDM5A* gene signature is associated with therapeutic response to patients with metastatic melanoma treated with anti–PD-1 antibody

To obtain mechanistic insights into the function of KDM5A and further understand the potential role of KDM5A in conferring clinical response to anti–PD-1 therapy, we analyzed gene expression microarray data of 703 primary cutaneous melanoma samples from the Leeds Melanoma Cohort (LMC) (*14*). We divided the samples into four quartiles ranked by their expression of *KDM5A* and identified the differentially expressed genes between the two quartiles with the highest and lowest expression (fig. S1A and data file S1A). Gene set enrichment analysis (GSEA) identified 20 gene signatures that were positively correlated with higher expression of *KDM5A* (data file S1B), among which two established gene signatures reactome PD-1 signaling (ranking 2nd) and reactome chromatin modifying enzymes (ranking 11th) were skewed toward high expression of *KDM5A* (Fig. 1, A and B). To delineate a *KDM5A* gene signature, we analyzed RNA-seq data of 473 cutaneous melanoma samples from The Cancer Genome Atlas (TCGA) project (*15*) and identified differentially expressed genes that were up-regulated in the quartile with the highest expression of *KDM5A*. We then integrated 1193 genes from the TCGA skin cutaneous melanoma (SKCM) cohort and 93 genes from the LMC that were positively correlated with *KDM5A* expression. We identified eight intersecting targets (*KDM5A*, *RIOK1*, *MVB12B*, *HMCN1*, *FAM13C*, *PDE1A*, *IKZF3*, and *ANO3*) and defined this eight-gene set as a *KDM5A* gene signature (Fig. 1C).

We tested the utility of this *KDM5A* gene signature in predicting responses to anti–PD-1 therapy in patients with metastatic melanoma. We analyzed RNA-seq data from two large published cohorts for which patients with metastatic melanoma were treated with anti–PD-1 therapy and clinical response data were available: the Liu *et al.* (*16*) cohort (n = 121) and the Riaz *et al.* (*17*) cohort (n = 32). We evaluated the ability of the *KDM5A* signature gene expression to differentiate between responders and nonresponders by single-sample GSEA using Signature score (S-score) (*18*). S-scores revealed that the *KDM5A* signature was differentially enriched between tumor groups in both cohorts and most patients with responding tumors had positive S-scores (Fig. 1D and fig. S1B).

We built predictive models of the response to ICB using the *KDM5A* gene signature in each cohort and compared their predictive accuracy, using area under the curve (AUC) analysis, to models built from published biomarker gene sets of response, including models that combined the *KDM5A* gene signature with the published biomarker sets. In addition to tumor mutational burden (TMB) (*19*), the gene expression–based biomarker sets that we evaluated were T cell–inflamed gene expression profile (GEP) (*20*), chemokine signature (*21*), Immunoscore (*21*), cytolytic activity (CYT) (*22*), major histocompatibility complex I (MHC-I) (*16*), and MHC-II (*16*) (data file S2). The *KDM5A* gene signature alone yielded an overall AUC accuracy of 0.65 with the Liu *et al.* (*16*) melanoma cohort and 0.63 with the Riaz *et al.* (*17*) cohort and showed similar or better performance compared to the other published biomarker gene sets (Fig. 1E and fig. S1C). Combining the *KDM5A* gene signature with some of the published biomarker sets improved the predictive accuracy, including TMB and T cell–inflamed GEP (Fig. 1E and fig. S1C). In addition, higher expression of *KDM5A* was associated with higher survival rate in the Liu *et al.* (*16*) cohort of 121 patients with metastatic melanoma, assessed by both overall survival and progression-free survival (Fig. 1, F and G). We repeated the analysis of the Liu *et al.* (*16*) cohort using a subset of the samples for which RNA-seq data were available before the patients receiving anti–PD-1 antibody treatment. With these pre–anti–PD-1 tumor samples (n = 104), we observed similar results for the predictive response value of the *KDM5A* gene signature and the positive correlations between overall and progression-free survival and high *KDM5A* expression (fig. S1, D to G). Collectively, our findings suggested that the *KDM5A* gene signature could potentially serve as a marker for ICB response.

KDM5A overexpression enhances anti–PD-1 therapy responses in mouse models of melanoma and colon cancer

Because we found that the *KDM5A* gene signature is associated with anti–PD-1 therapy response in melanoma, we explored whether increasing KDM5A improved the efficacy of anti–PD-1 blockade immunotherapy in mouse models. We selected the B16 melanoma model due to its primary resistance to ICB by an anti-mouse PD-1 antibody (*23*). We inoculated KDM5A-overexpressing B16 cells into wild-type mice and treated these mice with anti–PD-1 antibody. Anti–PD-1 antibody reduced tumor volume in mice bearing the B16 cells overexpressing KDM5A compared with that of mice treated with immunoglobulin G (IgG) antibody; however, no such reduction was observed for mice with wild-type B16 tumors (Fig. 1H). Moreover, we observed a similar effect of KDM5A overexpressing in the MC38 colon cancer model (Fig. 1I and fig. S1H). Thus, the combination of increased KDM5A and anti–PD-1 antibody outperformed anti–PD-1 antibody monotherapy in two mouse cancer models.

Another way to indirectly increase KDM5A-mediated histone regulation would be to inhibit the activity of an H3K4 methylase [mixed lineage leukemia protein-1 (MLL1)]. By preventing methylation, MLL1 inhibition would amplify the cellular consequences of KDM5A activity. We found that the combination of an anti–PD-1 antibody with MM102, an inhibitor of MLL1 (*24*), led to a reduction in the volume of B16 melanoma tumors in mice compared with tumor volumes of mice with IgG or either agent individually (fig. S1I, left). Similar results were observed in the MC38 colon cancer model (fig. S1I, right).

We also used the KDM5A inhibitor YUKA-2 (*25*) to test the role of KDM5A catalytic activity in augmenting the antitumor effects of anti–PD-1 antibody treatment. As anticipated, we did not observe

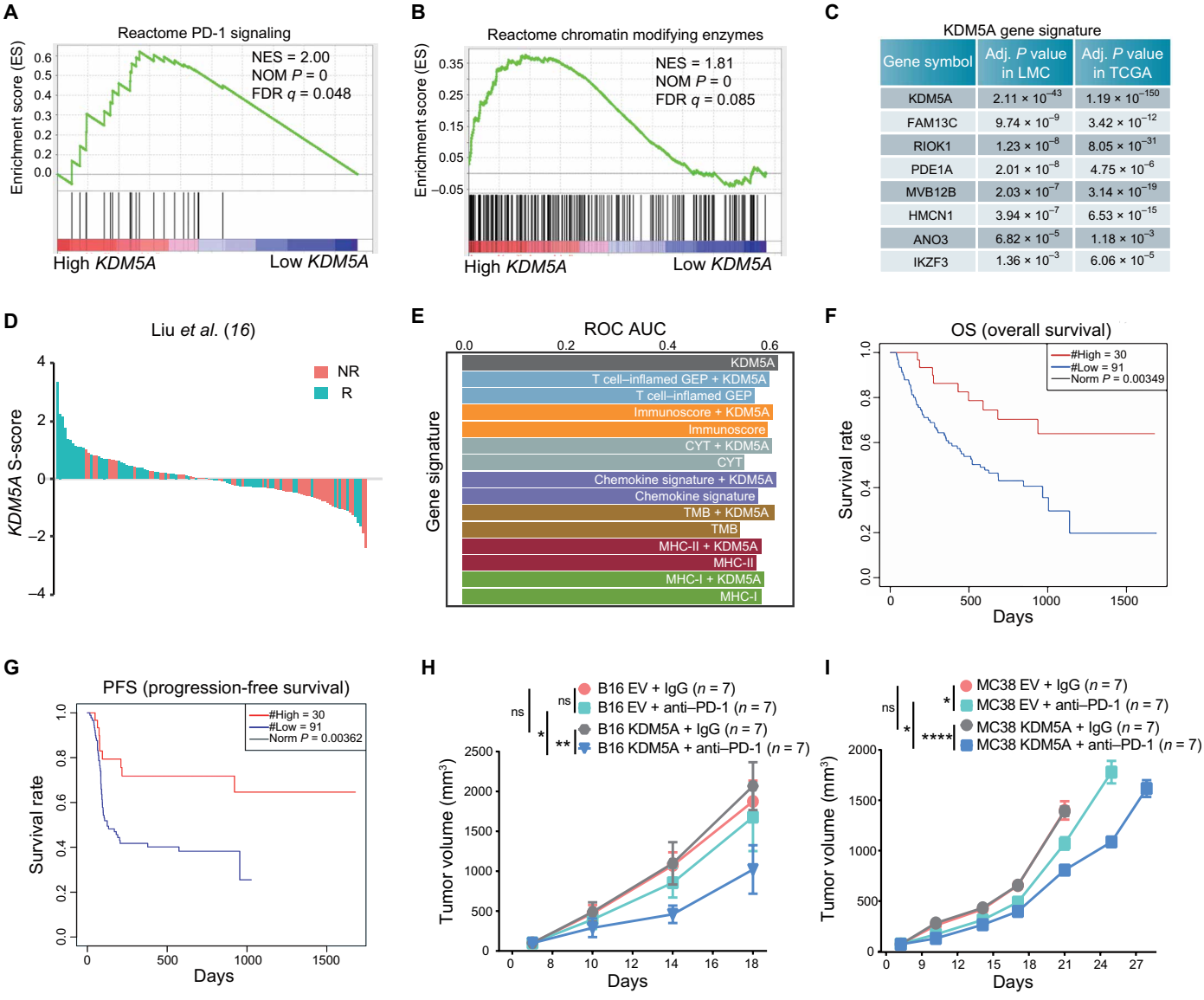

Fig. 1. A *KDM5A* gene signature is associated with therapeutic response of patients with metastatic melanoma treated with anti–PD-1 antibody. (**A** and **B**) GSEA plots of reactome PD-1 signaling and reactome chromatin modifying enzymes showing positively correlation with higher expression of *KDM5A* in the LMC. NES, normalized enrichment score; NOM, nominal; FDR, false discovery rate. (**C**) Table showing the *KDM5A* gene signature of eight genes that were significantly up-regulated in the subgroup of higher expression of *KDM5A* in both TCGA SKCM and LMCs. The cutoff criteria were $\log_2$ fold change > 0.75 and an adjusted P <0.05 for the LMC and $\log_2$ fold change > 1 and adjusted P <0.05 for the TCGA SKCM cohort. (**D**) A waterfall plot depicting the *KDM5A* Signature scores (S-score) for responder (R) and nonresponder (NR) in the Liu *et al.* (*16*) dataset (n = 121, Welch two-sample t test, P = 0.0004021) (*16*). Patients whose responses were complete response, partial response, stable disease, or mixed response responders were classified as responders; patients whose responses were progressive disease were classified as nonresponders. (**E**) Mean cross-validation AUC scores from models of the *KDM5A* gene signature and other published biomarkers used alone or in combination for predicting response to anti–PD-1 immunotherapy in the Liu *et al.* dataset (n = 121) (*16*). See data file S2 for genes in the signatures. ROC, receiver operating characteristic. (**F** and **G**) The Kaplan-Meier overall and progression-free survival of patients in the Liu *et al.* dataset (n = 121) (*16*) that was stratified by high versus low *KDM5A* S-score (split by the 75% quantile). Statistical significance was determined by two-sided Kaplan-Meier log-rank test. A number of patients in each *KDM5A* S-score group are indicated by #High and #Low. (**H**) Tumor volume of B16 or KDM5A-overpressing B16 (B16 KMD5A) melanoma subcutaneously inoculated in C57BL/6 mice treated with IgG control antibody or anti–PD-1 antibody as indicated. EV, empty vector. (**I**) Tumor volume of MC38 or KDM5A-overpressing MC38 (MC38 KDM5A) colon cancer subcutaneously inoculated in C57BL/6 mice treated with IgG control antibody or anti–PD-1 antibody as indicated. In (H) and (I), data are presented as the means ± SEM from one of two experiments. Tumor volume data were analyzed with two-way ANOVA (H and I). *P < 0.05, **P < 0.01, and ****P < 0.0001. ns, P > 0.05. See data file S3 for raw data for (D), (E), (H), and (I).

any enhanced antitumor effects when mice were treated with the combination of the KDM5A inhibitor and anti–PD-1 antibody (fig. S1J). The KDM5A inhibitor had no antitumor effect as a monotherapy. Collectively, these results supported our hypothesis that increasing KDM5A activity in tumor cells can boost the efficacy of anti–PD-1 blockade.

KDM5A binds at the *Pten* promoter and decreases *Pten* transcription to up-regulate PD-L1

Increased PD-L1 improves the efficacy of anti–PD-1 or PD-L1 immunotherapy (*26*, *27*). We therefore examined PD-L1 abundance in MC38 cells overexpressing KDM5A and observed a significant

increase in PD-L1 compared to wild-type MC38 cells ($P = 0.0036$; Fig. 2A). To investigate how KDM5A enhances PD-L1 abundance, we performed quantitative proteomics analysis of MC38 cells and observed that KDM5A overexpression markedly increased the abundance of 11 proteins and decreased the abundance of five proteins associated with the PI3K-AKT-S6K1 signaling cascade (Fig. 2B). Previous studies established that the tumor suppressor PTEN (phosphatase and tensin homolog) inhibits activity of the PI3K-AKT-S6K1 cascade in prostate cancer and this cascade promotes PD-L1 accumulation (*28*).

Because KDM5A is a histone demethylase, we performed chromatin immunoprecipitation (ChIP) coupled with quantitative PCR (qPCR) of MC38 cells. We found that KDM5A directly interacts with the *Pten* promoter (~3 kb proximal to the transcription start site) (Fig. 2C). Consistent with this finding, the amount of H3K4me3 was lower in the *Pten* promoter region in MC38 cells than in *Kdm5a*-knockout MC38 cells (Fig. 2C). We also used both qPCR and immunoblotting to confirm that overexpression of KDM5A reduced the abundance of PTEN at the transcript and protein levels in MC38 cells (Fig. 2, D and E). In addition, we analyzed a dataset from a large-scale ChIP sequencing study of mouse embryonic stem cells and found consistent evidence to support the direct binding interaction between KDM5A and the *Pten* promoter (*29*).

Previous studies have shown that treatment with PI3K and AKT inhibitors, or PTEN overexpression, reduces PD-L1 in tumors (*30*, *31*, *32*). We conducted a series of biochemical experiments with inhibitors of PI3K-AKT-S6K1 signaling proteins. In MC38 cells, inhibitor of PTEN (SF1670) increased PD-L1 abundance, whereas each inhibitor of the pathway PI3K (NVP-BKM120), AKT (MK2206), mammalian target of rapamycin (mTOR) (rapamycin), or S6K1 (PF-4708671) decreased PD-L1 abundance (fig. S2, A and B). The decrease of PD-L1 in cells exposed to the PI3K inhibitor (NVP-BKM120) or AKT inhibitor (MK2206) coincided with decreased activation of AKT and S6K1 (fig. S2C). Collectively, these results indicated the mechanism through which KDM5A up-regulates PD-L1: By binding at the *Pten* promoter, KDM5A decreased *Pten* transcription, thereby activating the PI3K-AKT-S6K1 signaling cascade.

D18 is a small molecule that increases KDM5A abundance for use in combination immunotherapy

Because we found that KDM5A increases the abundance of PD-L1 in tumor cells, we hypothesized that combining anti–PD-L1 with agents that increase KDM5A would induce an antitumor effect. We inoculated wild-type and KDM5A-overexpressing MC38 cells into mice and treated the mice with or without anti–PD-L1 antibody. Whereas anti–PD-L1 antibody monotherapy exerted little, if any, antitumor effect on wild-type MC38 tumors, this monotherapy caused a significant decrease in the growth of tumors from MC38 cells with increased KDM5A ($P = 0.0025$; Fig. 3A). There were no obvious differences in growth between untreated wild-type and KDM5A-overexpressing MC38 tumors (Fig. 3A). Thus, increased KDM5A, in combination with anti–PD-L1 antibody, slowed MC38 tumor growth.

Consequently, we initiated screens of two chemical compound libraries. Our first effort sought to identify compounds that increased the amount of both KDM5A and PD-L1 in mouse colon cancer (MC38) and human colon cancer (HT29) cells. After screening thousands of compounds (1154 Food and Drug Administration–approved drugs) by high-throughput RNA-seq–based high-throughput screening (HST2) (*33*) and further testing by fluorescence-activated cell sorting (FACS) analysis, we identified that 18 compounds that increased both KDM5A and PD-L1 in both MC38 and HT29 cells (fig. S3A). One of the drugs that we identified was palbociclib, a cyclin-dependent kinase 4 and 6 (CDK4/6) inhibitor (*26*, *34*). Palbociclib has been tested in numerous clinical trials for various cancers (*35*). We observed that palbociclib increased the abundance of both KDM5A and PD-L1 (fig. S3A). To determine whether palbociclib exerts a synergistic effect with anti–PD-1 antibody, we inoculated MC38 cells in mice and treated the mice with the combination of palbociclib and the anti–PD-1 antibody. We observed that the combination treatment markedly slowed tumor growth (fig. S3B). Thus, our data indicated that palbociclib may have multiple mechanisms of action: By inhibiting CDK4/6, this drug reduces cancer cell proliferation, and by inducing an increase in PD-L1, this drug can promote sensitivity to PD-1 blockers.

We had designed a library of small molecules acting as potent agonists of TLR7/8, and TLR7/8 agonists have shown beneficial effects when combined with ICB agents in animal cancer models (*36*, *37*). Thus, we decided to conduct a screen using our TLR7/8 agonist small-molecule library to identify pharmacological activators of KDM5A. In this screen, we found that a pyridopyrimidine derivative compound, D18, increased the accumulation of both KDM5A and PD-L1 in MC38 cells (Fig. 3, B and C, and fig. S3, C to E). Because TLR agonists enhance the efficacy of PD-1 or PD-L1 blockade in a mouse squamous cell carcinoma model (*38*), we hypothesized that D18 simultaneously triggers two independent effects on separate cell types: D18 increases the accumulation of both KDM5A and PD-L1 in tumors and activates TLR7 and inflammatory cytokine–mediated responses in immune cells.

We confirmed that D18 increased KDM5A demethylation activity in MC38 cells. Because histone demethylases function in the nucleus, we characterized the subcellular localization of KDM5A. Treatment of MC38 cells with D18 caused an increase in the abundance of KDM5A in both the cytoplasm and the nucleus (Fig. 3, D and E). Immunoblotting with antibodies against H3K4me2 and H3K4me3 showed that treatment with D18 reduced the extent of histone lysine methylation in MC38 cells (fig. S3F). Consistent with the effects on KDM5A, D18 reduced PTEN abundance and increased PD-L1 abundance in both human (HT29) and mouse (MC38) colon cancer cells (Fig. 3F and fig. S3G). We also performed quantitative proteomics analysis and found that treatment of MC38 cells with D18 increased the abundance of 11 proteins associated with the PI3K-AKT-S6K1 signaling cascade, suggesting that this cascade was activated (Fig. 3G). We found that D18 attenuated the effects of PI3K or AKT inhibitors (Fig. 3H) or PTEN overexpression (Fig. 3I), consistent with D18 activating the PI3K-AKT-S6K1 signaling cascade. To demonstrate the effect of D18 on PD-L1 depended on KDM5A regulation of *Pten*, we tested the efficacy of D18 on *Kdm5a*-knockout MC38 cells and observed no obvious reduction in PTEN abundance nor a strong increase in PD-L1 abundance even at the highest concentration tested (Fig. 3J), indicating that MC38 cells lacking KDM5A did not respond to D18 treatment. Thus, D18 increased KDM5A, which enhanced PI3K-AKT-S6K1 signaling and promoted PD-L1 accumulation.

We next examined the activity of D18 as a TLR7/8 agonist. We used HEK-Blue cells expressing specific TLRs and a reporter gene for nuclear factor κB (NF-κB) activity (a transcription factor activated by TLR signaling) (InvivoGen) for these experiments

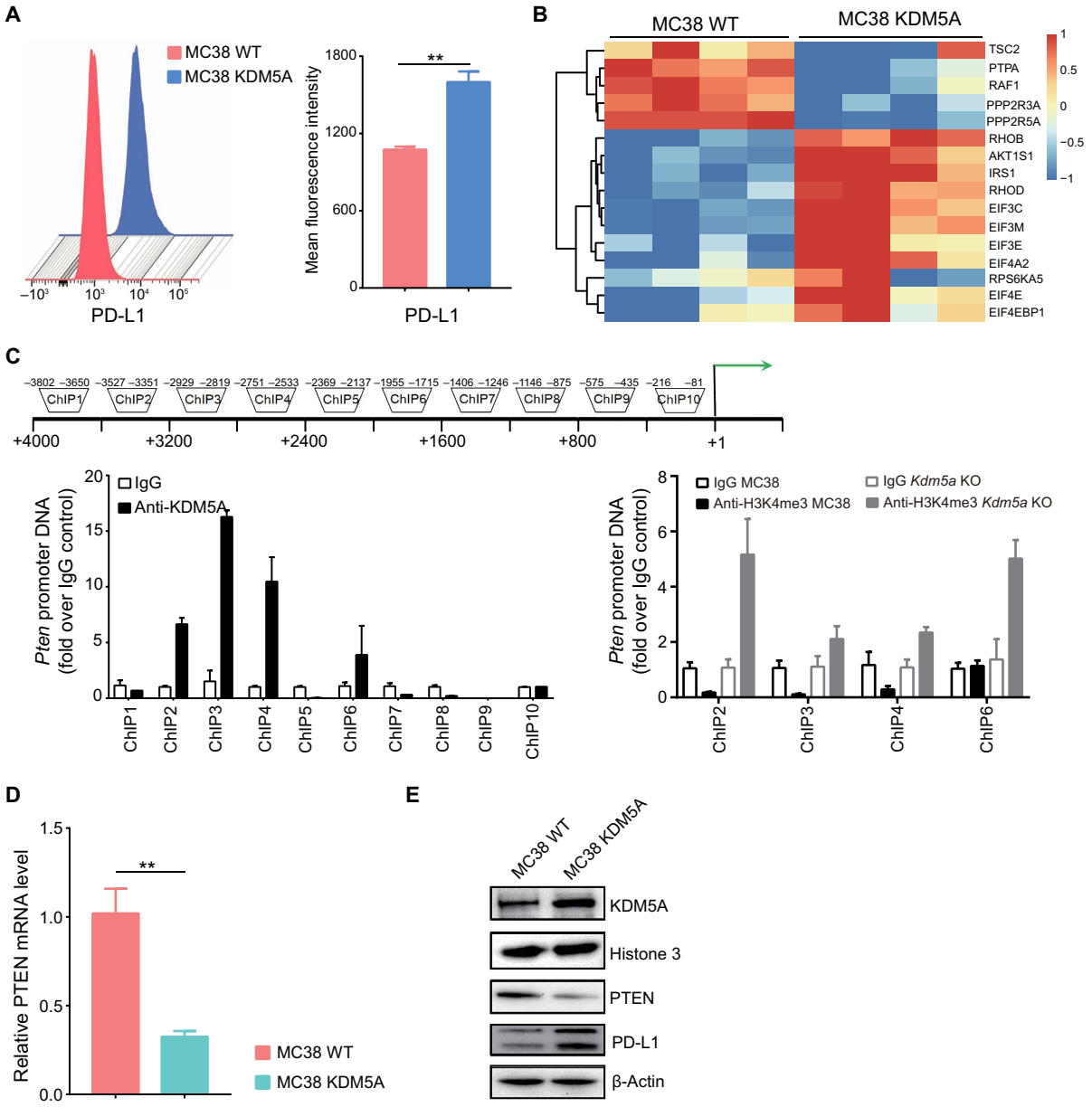

Fig. 2. KDM5A decreases PTEN abundance and increases PD-L1 abundance. (**A**) PD-L1 was visualized by flow cytometry on wild-type (WT) or KDM5A-overexpressing MC38 cells. One representative experiment of three is shown (left), and results of three independent experiments are presented as means ± SEM (right). *P* values were calculated using two-tailed unpaired *t* test. $^{**}P < 0.01$. (**B**) Heatmap of a hierarchical clustering of the proteins in the "PI3K-AKT-S6K1" cascade in the indicated MC38 cells. Data are from quantitative proteomic analysis data with proteins in the cascade determined by Proteome Discoverer Searching Algorithm (version 1.4). Cluster analysis was performed with DAVID bioinformatics resources. (**C**) Chromatin immunoprecipitation (ChIP) analysis of the *Pten* promoter in MC38 cells. Left: KDM5A binding. Right: H3K4me3 in wild-type and *Kdm5a* knockout (KO) cells. The data are presented as the means ± SEM ($n = 3$) from one of three experiments. (**D**) qPCR analysis of relative *Pten* mRNA expression in wild-type and KDM5A-overexpressing MC38 cells. The qPCR data were normalized to β-actin. Data are means ± SEM ($n = 3$) from one of three experiments. *P* values were calculated by unpaired two-tailed Student's *t* tests. $^{**}P < 0.01$. (**E**) Western blot analysis of wild-type and KDM5A-overexpressing MC38 cells with antibodies against the indicated proteins. Data are representative of one of three experiments. See data file S3 for raw data for (A) to (D).

because these cells enable efficient monitoring of TLR activity using NF-κB/activator protein 1 (AP-1)–inducible secreted embryonic alkaline phosphatase reporter systems. Treatment of the HEK-Blue cells with D18 resulted in activation of both the TLR7 and TLR8 signaling cascades: The half-maximal effective D18 concentration was 37 nM for TLR7 activation and 16.7 nM for TLR8 activation (fig. S3H). The commercial TLR7 agonist R848 was included as a positive control in these experiments. Furthermore, D18 did not activate signaling in HEK-Blue cells transfected with TLR2 or TLR4 (fig. S3I).

To confirm that treatment with D18 stimulates the expression of genes encoding inflammatory cytokines, we derived bone marrow–derived macrophages from wild-type and *Myd88* knockout mice and treated the macrophages with D18. MyD88-deficient macrophages are unresponsive to most known TLR ligands in terms of

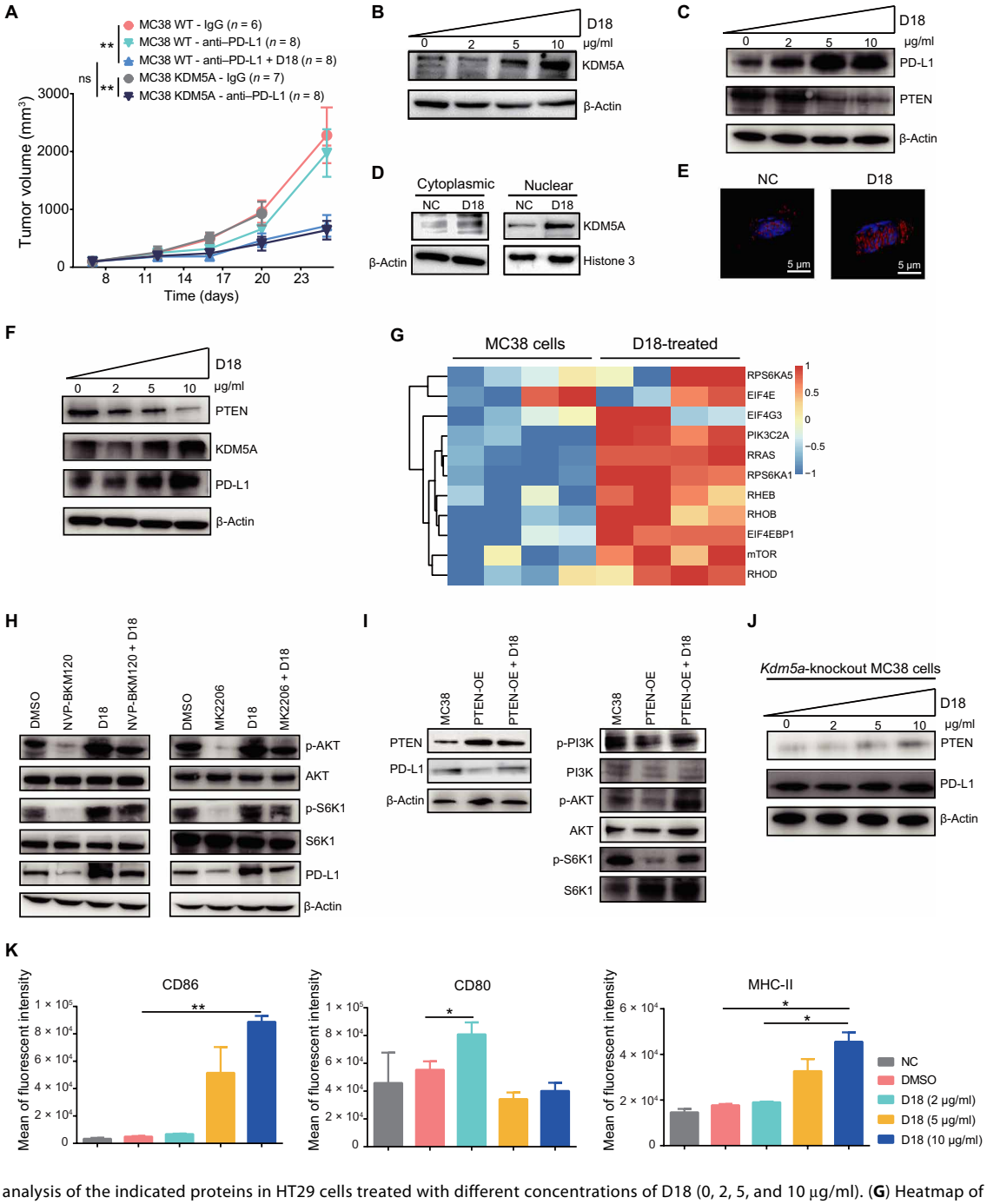

Fig. 3. A small-molecule activator of KDM5A (D18) increases PD-L1 abundance by activating PI3K-AKT-S6K1 cascade. (**A**) Mice bearing MC38 or KDM5A-overexpressing MC38 cells were divided into the indicated treatment groups, and the tumor volumes of mice treated with IgG control antibody, anti–PD-L1 monoclonal antibody, D18, or combined D18 and anti–PD-L1 antibody were measured and plotted. Data are presented as means ± SEM (six to eight mice per group) from one of two experiments. The tumor volumes of mice treated with IgG control antibody reached end point at day 23, and therefore, the mice were euthanized. Statistical significance was determined by two-way ANOVA. $^{**}P < 0.01$. ns, $P > 0.05$. (**B**) Western blot analysis of KDM5A abundance in MC38 cells treated with different concentrations of D18 (0, 2, 5, and 10 μg/ml). (**C**) Western blot analysis of PD-L1 and PTEN abundance in MC38 cells treated with different concentrations of D18. (**D**) Western blot analysis of KDM5A abundance in the nuclear and cytoplasmic fractions of MC38 cells treated with D18 (2 μg/ml) or with dimethyl sulfoxide (DMSO) as negative control (NC). (**E**) Representative immunofluorescence images of a single MC38 cell and D18-treated MC38 cell stained for KDM5A (red) and 4′,6-diamidino-2-phenylindole (DAPI) (blue). Scale bars, 5 μm. Data are representative of one from three independent experiments. (**F**) Western blot analysis of the indicated proteins in HT29 cells treated with different concentrations of D18 (0, 2, 5, and 10 μg/ml). (**G**) Heatmap of a hierarchical clustering of the proteins in the PI3K-AKT-S6K1 cascade in the indicated MC38 cells. Data are from quantitative proteomic analysis data with proteins in the cascade determined by Proteome Discoverer Searching Algorithm (version 1.4). Cluster analysis was performed with DAVID bioinformatics resources. (**H**) Western blot analysis of the indicated proteins and phosphorylated (p) proteins in MC38 cells treated with PI3K inhibitor (NVP-BKM120; 20 μM), AKT inhibitor (MK2206; 5 μM), D18 (2 μg/ml), or D18 combined with NVP-BKM120 or with MK2206 for 24 hours. (**I**) Western blot analysis of the indicated proteins and phosphorylated proteins in MC38 cells, PTEN-overexpressing (PTEN-OE) MC38 cells, and PTEN-overexpressing MC38 cells exposed to D18 (2 μg/ml for 24 hours). (**J**) Western blotting analysis of PTEN and PD-L1 in *Kdm5a*-knockout MC38 cells treated with different concentrations of D18 for 24 hours. (**K**) Quantification of flow cytometry data of CD86, CD80, and MHC-II abundance on mouse bone marrow-derived dendritic cells (BMDCs) treated with different concentrations of D18. NC is the no treatment negative control; DMSO is the vehicle control. Data are presented as the means ± SEM ($n = 3$) from one of three experiments. Statistical significance was calculated by unpaired two-tailed Student's *t* test. $^{*}P < 0.05$ and $^{**}P < 0.01$. Western blot data in (B), (C), (D), (F), (H), (I), and (J) each represent results from one of three experiments. See data file S3 for raw data for (A), (G), and (K).

cytokine production (*39*) and thus serve as a negative control. Wild-type macrophages treated with D18 expressed increased *Ifnα*, *Tnfα*, *Il6*, and *Il12b*, whereas the mRNAs for these cytokines were nearly undetectable in MyD88-deficient macrophages (fig. S3J). These results indicated that D18 activates macrophages in a MyD88-dependent manner. In addition, D18 increased the abundance of three cell surface activation markers (CD80, CD86, and MHC-II) in bone marrow–derived DCs (Fig. 3K). However, D18 had no effect on the abundance of CD80, CD86, or MHC-II in bone marrow–derived DCs from TLR7-deficient mice (fig. S3K). Collectively, these results indicated that D18 is a specific TLR7/8 dual agonist and activates macrophages and DCs, the latter through TLR7 in mouse.

Combination therapy with D18 and anti–PD-1 antibody is effective in treating mouse models of multiple cancer types

To evaluate whether treatment with D18 as a monotherapy or in combination with anti–PD-1 antibody can inhibit tumor growth, we performed in vivo studies with a syngeneic tumor model in which mice bearing MC38 tumors were treated with D18. Although D18 monotherapy did suppress tumor growth, the combination of D18 and anti–PD-1 antibody caused a more pronounced suppressive effect on tumor growth compared to mice treated with either single agent, assessed in terms of both tumor size (Fig. 4A) and animal survival (Fig. 4B). In MC38 tumors, we confirmed that D18 and the combination therapy induced an increase in both KDM5A and PD-L1 in $CD45^-$ cells, which exclude the immune cells and represent the cancer cells and possibly stromal cells in the tumor (fig. S4, A and B).

To determine whether the effect involved the ability of D18 to increase KDM5A and PD-L1 or to activate TLR7 or both, we treated *Myd88* knockout mice bearing MC38 tumors. The combination of D18 with anti–PD-1 antibody resulted in a stronger antitumor effect than either single agent (Fig. 4C), consistent with the induction of PD-L1 exerting a critical effect on anti–PD-1 antibody sensitivity. We also measured PD-L1 on $CD45^-$ cells in *Myd88* knockout mice and found that the increased PD-L1 abundance was induced by D18 (fig. S4C).

Furthermore, we used three more mouse models of different cancers to corroborate the efficacy of D18. These included the B16 (melanoma), 4T1 (breast cancer), and Ag104Ld (non–T cell–inflamed fibrosarcoma) cancer models. D18 enhanced the efficacy of anti–PD-1 antibody in the 4T1 mouse model (Fig. 4D), as well as in the B16 model (Fig. 4E), which is unresponsive to anti–PD-1 monotherapy treatment (*40*, *41*). D18 monotherapy was as effective as D18 and anti–PD-1 antibody combination therapy in suppressing tumor growth in Ag104Ld (Fig. 4F), suggesting that D18 may be a particularly efficacious agent for noninflamed tumors, which lack tumor-infiltrating T cells and have a low inflammatory signature (*42*).

Combination therapy with D18 and anti–PD-1 antibody promotes activation of both T helper 1 $CD4^+$ T cells and cytotoxic $CD8^+$ T cells

We evaluated how D18 and anti–PD-1 antibody combination treatment affects T cell responses or alters the TME or both. Compared to anti–PD-1 antibody or D18 monotherapy, the combination treatment increased the number of infiltrating $CD8^+$ T cells and raised the ratio of effector to regulatory T cells ($CD8^+$ T_{eff}/T_{reg}) in the three mouse cancer tumors we tested: MC38 (Fig. 5, A and B), 4T1 (fig. S5A), and Ag104Ld (fig. S5B). We characterized in detail the T cell profiles of the tumor-infiltrating immune cells in MC38 tumors. We detected an increased proportion of $IFN\gamma^+CD8^+$ T cells, representing the activated $CD8^+$ T cells, in MC38 tumors from mice treated with the combination treatment, whereas monotherapy with either anti–PD-1 antibody or D18 did not increase the proportion of $IFN\gamma^+CD8^+$ T cells (Fig. 5C). Compared with either monotherapy, the combination treatment increased the abundance of CD107a in $CD8^+$ T cells, indicating better cytotoxic T cell response (Fig. 5D). The combination treatment also markedly increased the proportion of $TNF\alpha^+CD8^+$ T cells (Fig. 5E), indicating that the cytotoxic function of $CD8^+$ T cells was activated.

To further confirm that the combination treatment promotes the activation of cytotoxic $CD8^+$ T cells, we performed RNA-seq of $CD8^+$ T cells ($CD45^+CD3^+CD8^+$ cells) isolated from MC38 tumors from mice treated with anti–PD-1 antibody or with D18 and anti–PD-1 antibody. We analyzed the expression of the killer lymphocyte effector genes and found that the genes encoding granzyme, interferon-γ (IFNγ), and tumor necrosis factor (TNF) were up-regulated by the combination treatment (fig. S5C). In addition, the abundance of T cell exhaustion markers in $CD8^+$ T cells, such as PD-1 and T-cell immunoglobulin mucin-3 (TIM-3), was decreased in MC38 tumors treated with the combination therapy compared to anti–PD-1 antibody monotherapy (fig. S5, D and E). This suggested that combination treatment improves the antitumor effects of ICB therapy by reducing the exhaustion of T cells.

RNA-seq profiling of $CD4^+$ T cells ($CD45^+CD3^+CD4^+CD25^-$ cells) showed that both the T helper 1 (T_H1) pathway and IFN signaling pathway were activated (fig. S6A). To verify this, we performed FACS analysis and found that MC38 tumors from mice treated with D18 and anti–PD-1 antibody had increased infiltration of two types of $CD4^+$ T cells (T-bet^+ cells and $CD107a^+$ T cells) (Fig. 5F). T-bet is a transcription factor required for T_H1 cell differentiation and IFN production (*43*). $CD107a^+$ T cells are a type of activated $CD8^+$ T cells (*44*). To further confirm the activation of effector T cells, we performed a Luminex bead assay to profile serum samples derived from mice bearing MC38 tumors and that were treated with D18 and anti–PD-1 antibody. We observed an increase in the amounts of the T_H1 cytokines interleukin-2 (IL-2), IL-6, IL-12, and IFNγ and another proinflammatory cytokine IL-17 but a decrease in the amount of the T_H2 cytokine IL-10 (fig. S6B). Collectively, these results indicated that the combination of D18 with anti–PD-1 antibody activates both T_H1 $CD4^+$ T and cytotoxic $CD8^+$ T cells.

Clonal expansion of particular T cell populations can be monitored on the basis of repertoires of T cell receptors (TCRs) (*45*, *46*). Increasing the number of infiltrating T cells and simultaneously improving the quality of the intratumoral TCR repertoire would effectively activate T cell immune responses and thereby benefit cancer therapy (*47*). We therefore examined whether combination treatment with D18 and anti–PD-1 antibody increased the clonality of tumor-specific T cells by analyzing the TCRβ subunit repertoires of T cells isolated from MC38 tumors using RNA-seq and based on a standard clonality index (1-normalized Shannon index). We found that D18 (0.5137 ± 0.0406), anti–PD-1 monotherapy (0.5820 ± 0.0078), and the combination treatment (0.5665 ± 0.0091) each increased the clonality compared with tumors from mice treated with IgG (Fig. 5, G and H). This suggested that either D18 or

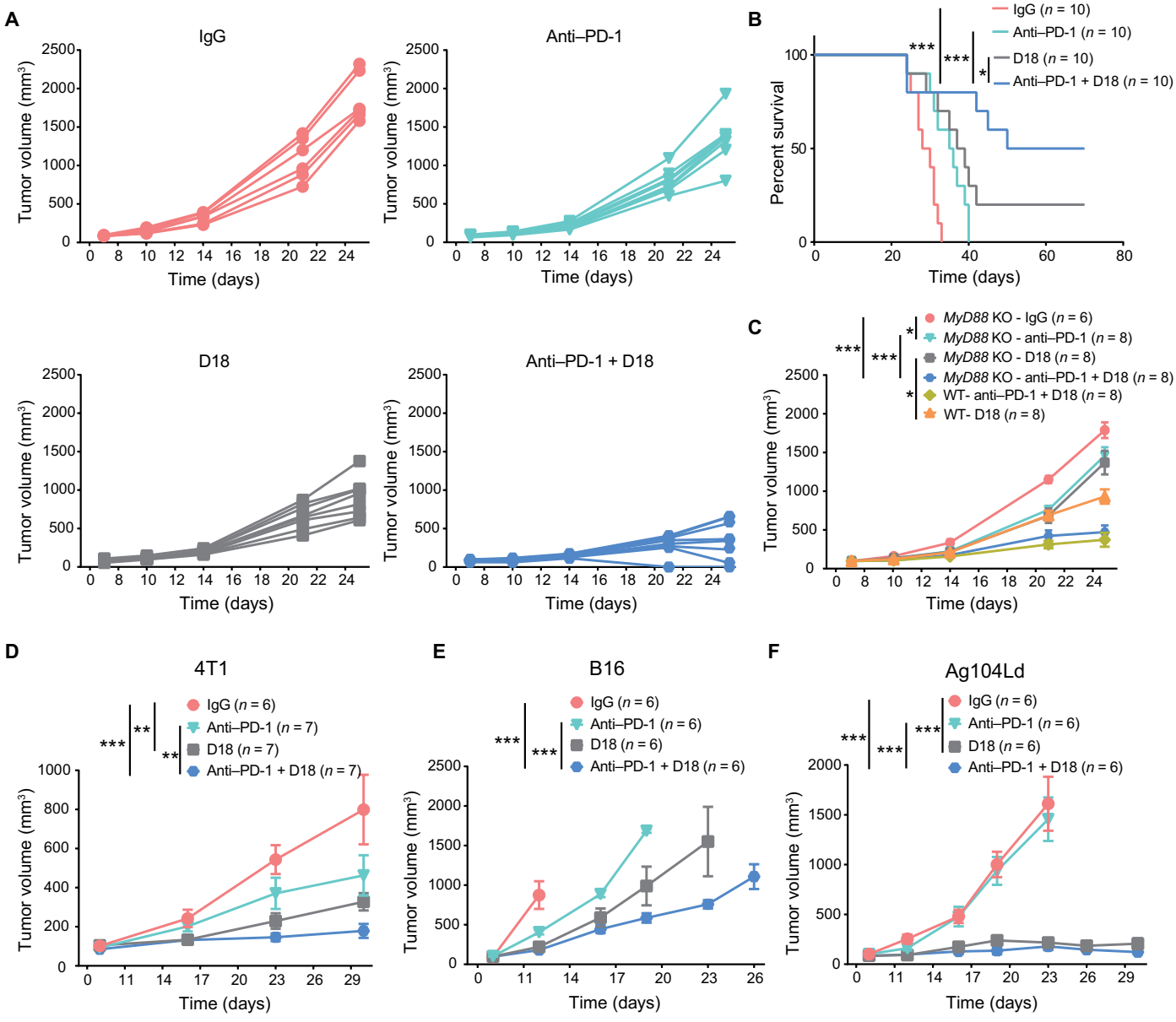

Fig. 4. Combination therapy with D18 and anti–PD-1 antibody is effective in treating mouse models of multiple cancer types. (**A** and **B**) Effect of monotherapy and combination anti–PD-1 and D18 on tumor-bearing (MC38 cells) mice. Mice were randomly divided into the treatment groups. Tumor volumes of mice treated with IgG control antibody, anti–PD-1 antibody, D18, or combined D18 and anti–PD-1 antibody ($n = 8$ mice for each group) were measured and plotted. Survival curves for each treatment group. Statistical significance was determined by log-rank (Mantel-Cox) test. $^*P < 0.05$ and $^{***}P < 0.001$. (**C**) MC38 tumor volumes from wild-type and *Myd88* knockout mice treated with IgG control antibody, anti–PD-1 antibody, D18, or combined D18 and anti–PD-1 antibody. (**D**) Tumor volume of subcutaneous 4T1 tumors in mice treated with IgG control, anti–PD-1, D18, or D18 and anti–PD-1 antibody. (**E**) Tumor volume of subcutaneous B16 tumors in mice treated with IgG control, anti–PD-1, D18, or D18 and anti–PD-1 antibody. (**F**) Tumor volume of subcutaneous Ag104Ld tumors in mice treated with IgG control, anti–PD-1, D18, or D18 and anti–PD-1 antibody. In (C) to (F), mice were randomly divided into treatment groups. Data are presented as means ± SEM of *n* mice, as indicated on each panel. Statistical significance was determined by two-way ANOVA. $^*P < 0.05$, $^{**}P < 0.01$, and $^{***}P < 0.001$. See data file S3 for raw data for all panels.

anti–PD-1 monotherapy or the combination increased the frequency of common TCR clones and contribute to T cell expansion.

Because stimulated immunological memory can lead to a prolonged antitumor response and prevent relapse in patients with cancer (*47*, *48*), we next assessed immune memory responses in the MC38 colon cancer and Ag104Ld non–T cell–inflamed fibrosarcoma models. We isolated the $CD8^+$ T cells from the spleen of mice bearing the tumors and administered monotherapy or combination therapy. Within the splenic $CD8^+$ T cell population, combination treatment with D18 and anti–PD-1 antibody increased the proportions of both $CD8^+$ T cells and central memory cells ($CD44^+CD62L^+$) but did not alter the proportion of effector memory T cells (Fig. 5I and fig. S6, C and D). Antigen-specific $CD8^+$ T cell clones derived from central memory T cells, but not those derived from effector

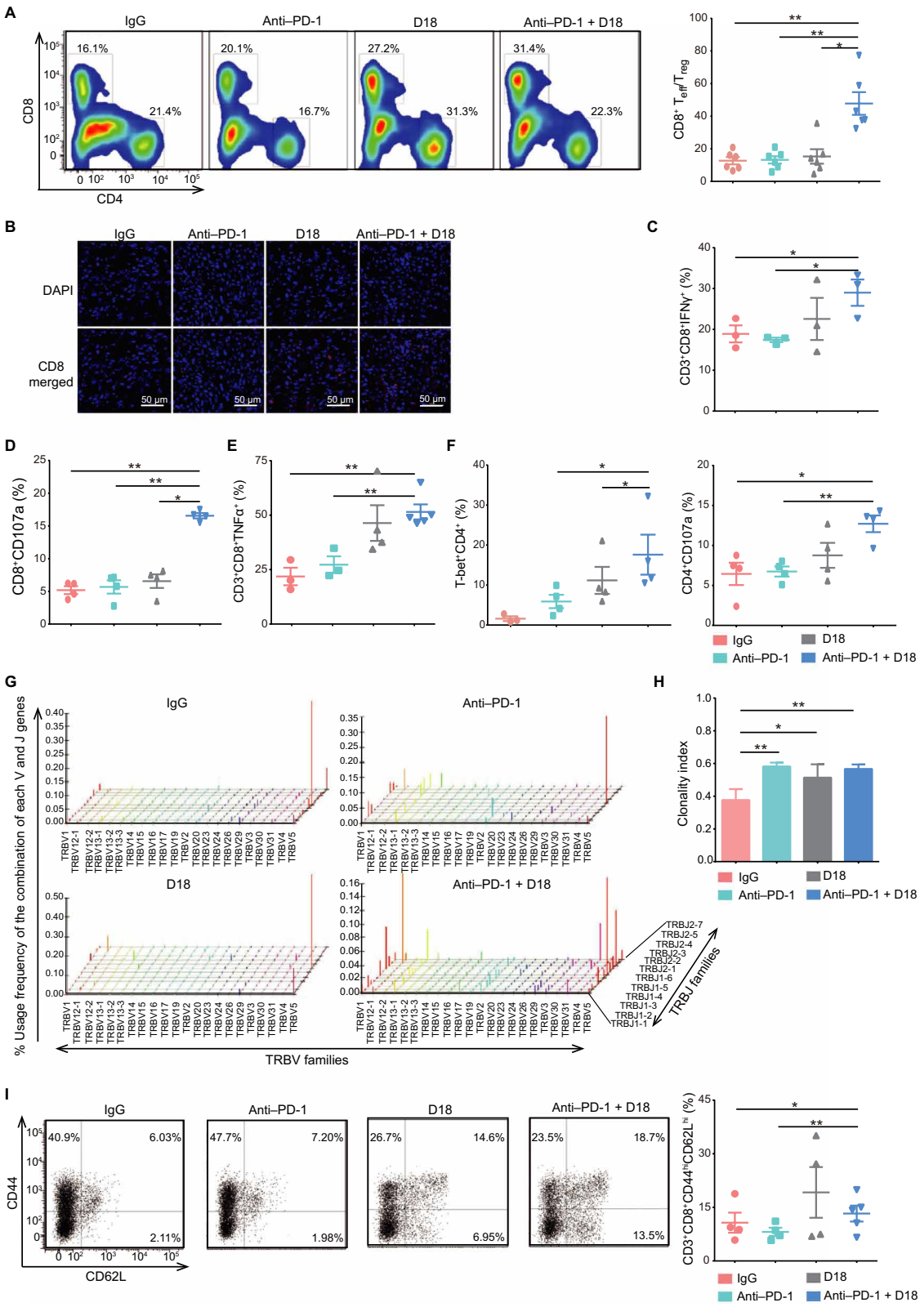

Fig. 5. Combination therapy with D18 and anti–PD-1 antibody promotes activation of both T_H1 $CD4^+$ T cells and cytotoxic $CD8^+$ T cells. (**A**) Representative flow cytometry analysis and quantification of $CD8^+$ T cells and the ratio of $CD8^+/T_{reg}$ ($CD4^+CD25^+$ $FoxP3^+$) in $CD45^+$ tumor-infiltrating lymphocytes (TILs) in MC38 tumors at day 33 of treatment: IgG control, anti–PD-1 antibody (200 μg per mouse), D18 (25 μg per mouse), and D18 and anti–PD-1 antibody. $n = 4$ to 6. (**B**) Immunofluorescence images of $CD8^+$ T cells in MC38 tumors analyzed by confocal microscopy. Representative images are shown. Scale bars, 50 μm. (**C** to **F**) Quantification by flow cytometry analysis of the indicated $CD8^+$ and $CD4^+$ TILs in MC38 tumors with the indicated treatments as described in (A). Symbols show data for each tumor ($n = 4$), and means ± SEM are indicated. (**G**) Representative TCR repertoire clonalities of T cells isolated from MC38 tumor–bearing mice with the indicated treatments as described in (A). The *x* and *y* axes show the combination of V and J genes (*TRAV* and *TRAJ* families), and the *z* axis shows their frequency of usage. (**H**) Clonality index of T cells in MC38 tumors from mice with the indicated treatments as indicated. Clonality index is shown as the 1-normalized Shannon index with higher values representing TCR clonal expansion. Data are means ± SEM from three tumors per condition as described in (A). (**I**) Representative flow cytometry analysis and quantification of double-negative T cells (T_{DN}) ($CD44^-CD62L^-$), naive T cells (T_N) ($CD44^-CD62L^+$), effector memory T cells (T_{EM}) ($CD44^+CD62L^-$), and central memory T cells (T_{CM}) ($CD44^+$ $CD62L^+$) populations on the $CD8^+$ T cells of spleens of MC38 tumor–bearing mice with the treatments as indicated. Symbols show data for each tumor ($n = 4$), and means ± SEM are indicated. For (A) to (I), statistical significance was determined by unpaired two-tailed Student's *t* tests. $^*P < 0.05$ and $^{**}P < 0.01$. See data file S3 for raw data for (G) and (H).

memory T cells, can persist for a particularly long duration in vivo (*49*). Thus, our data indicated that combination treatment increases central memory T cells and thereby generates memory antitumor immune responses. We conducted rechallenge experiments using the MC38 colon cancer and Ag104Ld non–T cell–inflamed fibrosarcoma models with D18 and anti–PD-1 antibody combination therapy and found that tumor-free survivor mice were resistant to tumor reimplantation (fig. S6, E and F). These results suggested that this combination therapy can confer long-lasting adaptive immunity.

Combination therapy with D18 and anti–PD-1 antibody increases tumor-infiltrating CD103$^+$ DCs and M1 macrophages

Because we observed an increase in tumor-infiltrating T cells, we examined the abundance of positive and negative regulators of T cell recruitment. Activation of β-catenin signaling reduces the infiltration of T cells to the tumor, whereas the chemokines CXCL9 and CXCL10 have the opposite effect (*50*, *51*). We measured their abundance at the protein and mRNA levels in MC38 tumors. Immunohistochemistry and immunofluorescence staining showed that D18 and anti–PD-1 antibody combination treatment decreased β-catenin but increased the chemokines CXCL9 and CXCL10 (Fig. 6, A and B). We observed a similar effect at the mRNA level (Fig. 6C).

Aberrant β-catenin signaling inhibits the expression of the gene encoding CCL4, a chemokine that mediates trafficking of CD103$^+$ DCs to tumors (*50*). Therefore, it was expected that we detected increased CCL4 protein and transcript abundance in MC38 tumors with combination treatment (Fig. 6, A and C). As key antigen-presenting cells, DCs are important for stimulating of tumor-infiltrating T cells. Thus, we performed FACS analysis to measure the DC populations in three mouse cancer models (colon cancer, breast cancer, and non–T cell–inflamed fibrosarcoma). We found that D18 monotherapy and the D18 and anti–PD-1 antibody combination increased the proportion of CD103$^+$ tumor-infiltrating DCs in MC38 (Fig. 6D) and Ag104Ld tumors (fig. S7A) but not in 4T1 tumors (fig. S7B). RNA-seq analysis of CD103$^+$ DCs isolated from MC38 tumors demonstrated that the combination treatment increased the expression of IFN-related and antigen-presenting machinery–related genes, consistent with the FACS findings (fig. S7C).

We also evaluated the macrophage cells (CD11b$^+$F4/80$^+$) in the tumors from each of the three mouse cancer models. M1 macrophages suppress tumor growth by phagocytosis and by secreting inhibitory factors (*52*), whereas M2 macrophages promote tumor progression (*53*). In all three models, we found that the combination treatment expanded the inflammatory M1 macrophage population (CD11b$^+$F4/80$^+$MHC-II$^+$CD206$^-$) (Fig. 6E, left, and fig. S7, D and E). In the MC38 tumor model, we observed reduced M2 macrophages (CD11b$^+$F4/80$^+$MHC-II$^-$CD206$^+$) in response to the combination therapy (Fig. 6E). Thus, it appeared that combination treatment with D18 and anti–PD-1 antibody reprograms M2 macrophages into M1 macrophages, a finding consistent with studies reporting an M2-to-M1 shift in response to a TLR7 agonist (*38*, *54*).

D18 enhanced the antitumor effects when combination with both anti–PD-1 and anti–TIM-3 antibodies

To determine whether D18 can enhance the efficacy of any other ICB therapies, we tested anti–TIM-3 antibody in combination with D18. A previous study reported that dual targeting of both PD-1 and TIM-3 had a synergistic effect on reducing tumor growth (*55*). We therefore treated both MC38 and B16 tumor models with six different dual- or triple-combination treatments involving D18, anti–PD-1 antibody, and anti–TIM-3 antibody. We observed that D18 consistently increased the antitumor efficacies of these ICB antibodies (Fig. 7, A and B). We analyzed tumor-infiltrating lymphocytes in MC38 tumors. The triple therapy of D18, anti–PD-1 antibody, and anti–TIM-3 antibody expanded the population of CD8$^+$ T cells (Fig. 7C). Although the triple therapy did not affect the population of the T_{reg} cells (CD3$^+$CD4$^+$CD25$^+$Foxp3$^+$), it increased the T_{eff}/T_{reg} ratio (Fig. 7C). In addition, the triple therapy increased CD103$^+$ DCs and M1 macrophages (Fig. 7, D to E). Thus, D18 can be combined with different ICB agents to improve their therapeutic effects.

DISCUSSION

Our study demonstrated that increased KDM5A in tumor cells suppresses the expression of *Pten* and thereby increases the abundance of PD-L1, which, in turn, improves the efficacy of a variety of ICB drugs in mouse models of colon cancer and melanoma. We also showed that the small-molecule D18, which both increases KDM5A activity and is a TLR7/8 agonist, promotes antitumor T cell immunity and sensitizes tumors to PD-1 blockade. Our findings indicated a complex effect of D18 on both cancer cells and the tumor immune cell environment that enhances the efficacy of ICB agents (fig. S8). These findings suggest the enticing possibility that D18 may convert noninflamed tumors into inflamed tumors (*56*).

Our GSEA and predictive model analysis of two published cohorts also suggested that a *KDM5A* gene signature (eight-gene set) could serve as a potential marker of clinical response to anti–PD-1 therapy in melanoma. We also experimentally validated that increased KDM5A in tumor cells had no effect on tumor growth and rendered both B16 and MC38 tumors more responsive to anti–PD-1 antibody therapy. We propose that KDM5A gene expression or protein abundance may also be a marker of response to anti–PD-1/PD-L1 therapy in multiple cancers. With additional data, KDM5A abundance could also serve as a readout for screening small molecules for potential combination therapy with ICB agents.

KDM5A may have multiple mechanisms for promoting PD-L1 abundance. We showed that KDM5A increased the abundance of PD-L1 in tumor cells through a pathway suppression of PTEN expression and induction of PI3K-AKT-S6K signaling. How other H3K4 (de)methylases regulate PD-L1 abundance remains less clear. A study reported that the H3K4 methyltransferase MLL1 directly decreases the H3K4me3 amount in the *Cd274* (PD-L1–encoding gene) promoter and thereby decreases PD-L1 expression in pancreatic cancer cells (*57*). We believe that H3K4 (de)methylation might regulate PD-L1 abundance through different mechanisms in different cell types. Further studies are needed to establish how the epigenetic regulatory functions of H3K4me3 (de)methylases lead to changes in the abundance of proteins that are not encoded by direct gene targets of the demethylases.

In clinical trials, most progressing patients with on-treatment biopsies showed a lack of PD-L1 up-regulation in tumors with little or no infiltrated effector T cells (*58*, *59*). Thus, there is a correlation between clinical response and PD-L1 abundance in tumors. Our data suggested that the abundance of PD-L1 on tumor cells is essential

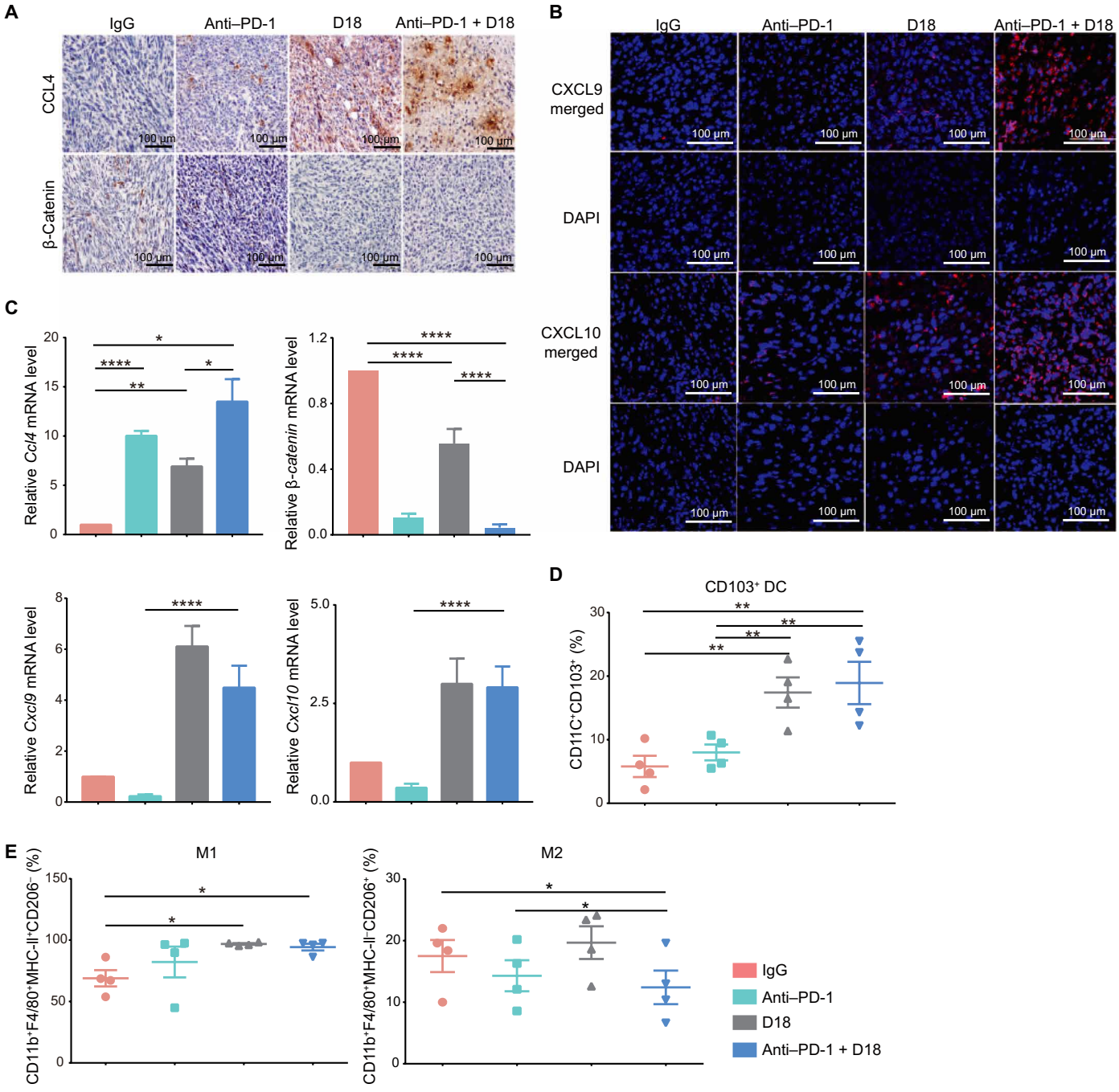

Fig. 6. Combination therapy with D18 and anti–PD-1 antibody increases M1 macrophages and tumor-infiltrating CD103$^+$ DCs. (**A**) Immunohistochemistry analysis of CCL4 and β-catenin in MC38 tumors from mice receiving IgG control, anti–PD-1, D18, or D18 and anti–PD-1 antibody as described in Fig. 5A. (**B**) Immunofluorescence analysis of CXCL9 and CXCL10 in MC38 tumors from mice receiving the indicated treatments as described in Fig. 5A. Representative images are shown. Scale bars, 100 μm. (**C**) qPCR analysis of *Ccl4*, *β-catenin*, *Cxcl9*, and *Cxcl10* mRNA in MC38 tumors from mice receiving the indicated treatments as described in Fig. 5A. The qPCR data were normalized to *Gapdh*. Each treatment group contained four to six mice. (**D**) Quantification of flow cytometry results of CD103$^+$ DCs in MC38 tumors from mice receiving the indicated treatments as described in Fig. 5A. (**E**) Quantification of flow cytometry results of M1-type macrophages (CD11b$^+$F4/80$^+$MHC-II$^+$CD206$^-$) and M2-type macrophages (CD11b$^+$F4/80$^+$MHC-II$^-$CD206$^+$) in MC38 tumors from mice receiving the indicated treatments as described in Fig. 5A. (C to E) Shown symbols represent individual tumors from a single mouse, along with means ± SEM. Statistical significance was calculated by unpaired two-tailed Student's *t* tests. *P < 0.05, **P < 0.01, and ****P < 0.0001. See data file S3 for raw data for (C).

for PD-1/PD-L1 blockade immunotherapy. We found that increasing PD-L1 abundance confers sensitivity to ICB agents in murine cancer models, which is consistent with the clinical observations (*58*, *59*). However, we cannot definitively exclude the possibility that PD-L1 on immune cells contributes to the efficacy of PD-1/PD-L1 blockade (*13*, *60*, *61*). It has been reported that the MHC-I

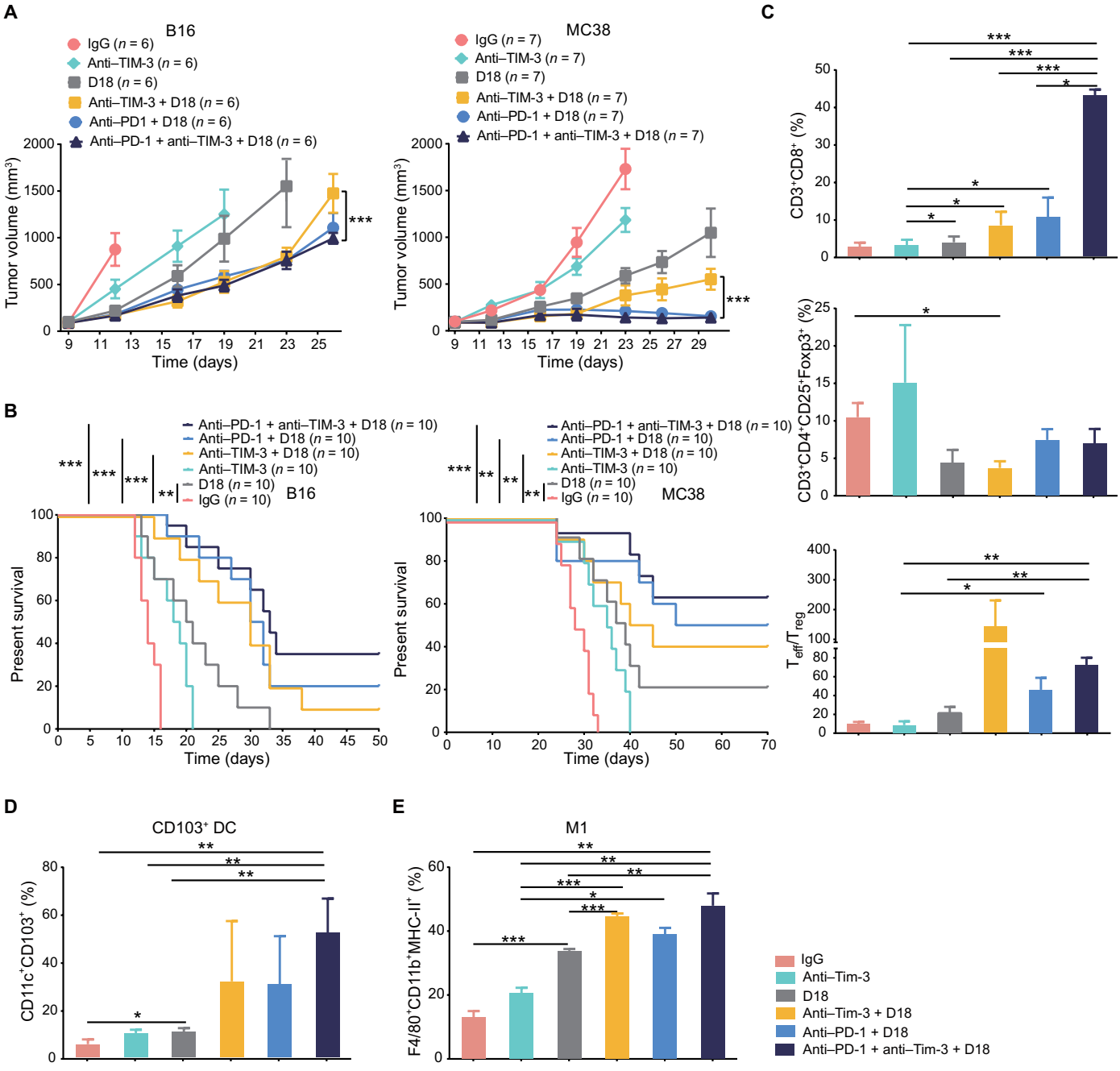

Fig. 7. D18 enhanced the antitumor effects of anti–PD-1 and anti–TIM-3 antibody combination therapy. (**A**) Tumor volume of subcutaneous B16 or MC38 tumors from mice receiving anti–TIM-3 (200 μg per mouse) and/or anti–PD-1 (200 μg per mouse) in combination with D18 (25 μg per mouse) or IgG control. Data are presented as means ± SEM for the indicated number of mice per treatment. Statistical significance was determined by two-way ANOVA. ***$P < 0.001$. (**B**) Survival at day 50 for B16 and day 70 for MC38 from mice receiving the indicated treatments as described in (A). Statistical significance was determined by log-rank (Mantel-Cox) test for the indicated number of mice per treatment. **$P < 0.01$ and ***$P < 0.001$. (**C**) Quantification of flow cytometry results of $CD8^+$ T cells in MC38 tumors on day 21 from mice receiving the indicated treatments as described in (A) ($n = 3$ to 5 mice). (**D**) Quantification of flow cytometry results of $CD103^+$ DC in MC38 tumors on day 21 from mice receiving the indicated treatments as described in (A) ($n = 3$ mice). (**E**) Flow cytometric analysis of expression of MHC-II (M1) in $CD11b^+F4/80^+$ cell populations on day 21 from mice receiving the indicated treatments as described in (A) ($n = 3$). In (C) to (E), data are presented as means ± SEM of the indicated number of mice per group. Statistical significance was determined by unpaired two-tailed Student's *t* tests. *$P < 0.05$, **$P < 0.01$, and ***$P < 0.001$. See data file S3 for raw data for all panels.

β_2-microglobulin–negative phenotype was associated with lack of PD-L1 tumor expression in patients with advanced non-small cell lung cancer (*62*) and that MHC-I mediated the cytosolic or endogenous neoantigen presentation to increase the tumor immunogenicity (*63*). To further identify the precise role of KDM5A or PD-L1 of tumor cells on cancer immunotherapy, first, answering how KDM5A or

PD-L1 expression regulates MHC-I expression on tumor cells is important, and additional investigation will be needed to resolve this issue.

In addition to evaluating cancer cell–intrinsic mechanisms for improving ICB agent responsiveness, we also examined tumor immune cell profiles (T cells, DCs, and macrophages) in mice treated with D18. We found an increase in both T-bet$^+$CD4$^+$ cells and CD4$^+$CD107a$^+$ T cells, in MC38 tumors from mice treated with D18 and anti–PD-1 antibody treatment. These results are consistent with studies, showing that T-bet is a master regulatory transcription factor involved in promoting the development of T_H1 CD4$^+$ T cells and inhibiting the T_H2 program (*64*, *65*). We also showed that D18 increases the numbers of DCs in the TME. DCs in tumors might present tumor antigens and thus contribute to activating T cells, but the precise functional relationship between antigen presentation of DCs and D18 is unknown. It will be interesting to determine whether D18 enhances antigen presentation of DCs, thus expanding the T cell immune response, and whether the D18-induced increase in KDM5A is involved.

M1 macrophages, positive for both MHC-I and MHC-II molecules and secreting high amounts of proinflammatory cytokines, are considered immunostimulatory inhibit tumor growth (*66*). Our data showed that D18 monotherapy increased M1 macrophages in the TME and decreased tumor size, an effect that was enhanced when combined with anti–PD-1 antibody in multiple cancer models (colon cancer, breast cancer, and non–T cell–inflamed fibrosarcoma). These findings are consistent with those from other studies, showing that improved patient survival is associated with increased numbers of M1 macrophages (*67*). We speculate that D18 promotes M2-to-M1 macrophage switching by enhancing the histone demethylation activity of KDM5A. High *KDM5A* expression by macrophages has been reported (*68*, *69*).

Regarding the limitations of this study, we have not ascertained how D18 increases KDM5A protein abundance or if D18 affects the abundance of other chromatin-modifying enzymes. Our ongoing efforts to address this question have included, for example, quantitative proteomics analysis of MC38 and D18-treated MC38 cells. D18 increased the abundance of 20 proteins and decreased the abundance of one protein associated with *KDM5A* expression. Another limitation is that we only investigated the KDM5A epigenetic target *Pten*. Other genes are likely targets of KMD5A-mediated histone demethylation, and other nonhistone proteins could also be KMD5A targets. We are performing experiments to determine the direct target proteins and genes of KDM5A.

In summary, our study establishes an empirical basis for developing the bifunctional small-molecule D18 as a combination agent for cancer therapies with anti–PD-1, anti–PD-L1, or anti–TIM-3. Given the ability of D18 to increase both KDM5A and PD-L1 abundance, its ability to induce TLR7/8 activation, and our data showing that this small molecule is an effective combination agent for use with multiple ICB agents, we propose that D18 represents an effective addition to cancer immunotherapy. In addition, increased *KDM5A* expression and the KDM5A gene signature could serve as potential markers for anti–PD-1 therapy response in melanoma patients.

MATERIALS AND METHODS

Study design

Our objective was to develop a combination agent with ICB for cancer therapy. Using analysis of publicly available RNA-seq data for tumors and cancer mouse models, we determined that elevated KDM5A in tumors improves the efficacy of anti–PD-1 treatment. We elucidated the mechanism of how KDM5A up-regulates PD-L1 expression in MC38 cells. We screened and identified a small molecule (D18) that can simultaneously increase KDM5A expression and activate TLR7/8. Last, we demonstrated the efficacy of D18 combined with anti–PD-1 antibody in mouse models of different cancers and the underlying immunologic mechanism. In all experiments, mice were randomly assigned to treatment groups after tumors were established. To ensure statistical power, 4 to 10 mice were included in each group, which enabled us to statistically distinguish tumor sizes and survival rates across groups. The samples size and statistical tests are described in each figure legend. Data include all outliers. Researchers were not blinded during treatment but were blinded during data collection and evaluation of the in vivo experiment. Experimental replicates were variable for each experiment and are indicated in the figure legend.

In vivo mouse studies

All mice were housed according to the guidelines of Tsinghua University Laboratory Animal Research Center and Animal Care and Use Committee. All animals were maintained under pathogen-free conditions and cared for in accordance with the International Association for Assessment and Accreditation of Laboratory Animal Care policies and certification. Six-week-old female C57BL/6 mice were purchased from Vital River (China).

Six-week-old C57BL/6 female mice were subcutaneously injected in the right flank with tumor cells (1×10^6 cells for the MC38 model, 2×10^5 for the B16 model, 2×10^5 for the 4T1 model, and 2×10^5 for the Ag104Ld model). Mice were pooled and randomly divided into different groups with a comparable average tumor size of 100 mm^3 ($1/2ab^2$, where a represents long diameter and b represents short diameter of tumor). D18 (25 μg per mouse) was administered once each week. IgG isotype control antibody, anti–PD-1 antibody, or anti–PD-L1 antibody (200 μg per mouse) was injected intraperitoneally twice each week. Palbociclib (100 mg/kg; diluted in 50 nM sodium D-lactate) was administered daily by oral gavage. Tumors were measured every 3 to 4 days. Mice that had no visible or palpable tumors that could be measured on consecutive measurement days were considered as "complete regressions." Animals were euthanized if they exhibited signs of distress or when the total tumor size reached 2500 mm^3. For the rechallenge study, tumor-free mice (complete regression) from the D18 and anti–PD-1 antibody group were rechallenged by subcutaneous intraperitoneal injection of 1×10^6 MC38 cells or 2×10^5 Ag104Ld cells on the contralateral side (left side). Wild-type C57BL/6 mice without subcutaneous intraperitoneal injection of tumor cells were used as negative controls. Tumor size was measured as described above.

Statistical analysis

To estimate the statistical significance of differences between two groups, we used unpaired Student's t tests to calculate two-tailed P values. A two-way analysis of variance (ANOVA) was performed when more than two groups were compared. Survival analysis was performed using Kaplan-Meier curves and evaluated with log-rank Mantel-Cox tests. Error bars indicate the SEM, unless otherwise noted. P values are labeled in the figures. P values were denoted as follows: $^*P < 0.05$, $^{**}P < 0.01$, $^{***}P < 0.001$, and $^{****}P < 0.0001$. Statistical analyses were performed by using GraphPad Prism (version 7.0).

SUPPLEMENTARY MATERIALS

stm.sciencemag.org/cgi/content/full/12/560/eaax2282/DC1
Materials and Methods
Fig. S1. Increased KDM5A improves the efficacy of anti–PD-1 blockade immunotherapy.
Fig. S2. Blocking PI3K-AKT-S6K signaling decreases PD-L1 abundance in MC38 cells.
Fig. S3. Development of a small molecule that increases KDM5A abundance for use in combination immunotherapy.
Fig. S4. The presence of KDM5A and PD-L1 on $CD45^-$ cells in MC38 tumors.
Fig. S5. Combination therapy with D18 and anti–PD-1 antibody promotes activation of cytotoxic $CD8^+$ T cells.
Fig. S6. Combination therapy with D18 and anti–PD-1 antibody promotes activation of T_H1 $CD4^+$ T cells and increases central memory cells in the spleen.
Fig. S7. Combination therapy with D18 and anti–PD-1 antibody increases tumor-infiltrating $CD103^+$ DCs and M1 macrophages.
Fig. S8. Schematic for the mechanisms by which D18 improves responses to anti–PD-1/anti–PD-L1 antibody.
Table S1. DNA oligo sequences used in this study.
Data file S1. The differentially expressed genes and top 20 gene signatures in LMCs.
Data file S2. Genes in the *KDM5A* gene signature and other published biomarker sets.
Data file S3. Original data.
References (*70*–*77*)

View/request a protocol for this paper from *Bio-protocol*.

REFERENCES AND NOTES

1. O. Hamid, C. Robert, A. Daud, F. S. Hodi, W. J. Hwu, R. Kefford, J. D. Wolchok, P. Hersey, R. W. Joseph, J. S. Weber, R. Dronca, T. C. Gangadhar, A. Patnaik, H. Zarour, A. M. Joshua, K. Gergich, J. Elassaiss-Schaap, A. Algazi, C. Mateus, P. Boasberg, P. C. Tumeh, B. Chmielowski, S. W. Ebbinghaus, X. N. Li, S. P. Kang, A. Ribas, Safety and tumor responses with lambrolizumab (anti-PD-1) in melanoma. *N. Engl. J. Med.* **369**, 134–144 (2013).
2. J. R. Brahmer, S. S. Tykodi, L. Q. Chow, W. J. Hwu, S. L. Topalian, P. Hwu, C. G. Drake, L. H. Camacho, J. Kauh, K. Odunsi, H. C. Pitot, O. Hamid, S. Bhatia, R. Martins, K. Eaton, S. Chen, T. M. Salay, S. Alaparthy, J. F. Grosso, A. J. Korman, S. M. Parker, S. Agrawal, S. M. Goldberg, D. M. Pardoll, A. Gupta, J. M. Wigginton, Safety and activity of anti-PD-L1 antibody in patients with advanced cancer. *N. Engl. J. Med.* **366**, 2455–2465 (2012).
3. D. S. Chen, I. Mellman, Elements of cancer immunity and the cancer-immune set point. *Nature* **541**, 321–330 (2017).
4. A. C. Palmer, P. K. Sorger, Combination cancer therapy can confer benefit via patient-to-patient variability without drug additivity or synergy. *Cell* **171**, 1678–1691.e13 (2017).
5. H. Santos-Rosa, R. Schneider, A. J. Bannister, J. Sherriff, B. E. Bernstein, N. C. Emre, S. L. Schreiber, J. Mellor, T. Kouzarides, Active genes are tri-methylated at K4 of histone H3. *Nature* **419**, 407–411 (2002).
6. R. J. Klose, Q. Yan, Z. Tothova, K. Yamane, H. Erdjument-Bromage, P. Tempst, D. G. Gilliland, Y. Zhang, W. G. Kaelin Jr., The retinoblastoma binding protein RBP2 is an H3K4 demethylase. *Cell* **128**, 889–900 (2007).
7. J. Cao, Z. Liu, W. K. Cheung, M. Zhao, S. Y. Chen, S. W. Chan, C. J. Booth, D. X. Nguyen, Q. Yan, Histone demethylase RBP2 is critical for breast cancer progression and metastasis. *Cell Rep.* **6**, 868–877 (2014).
8. L. P. Blair, J. Cao, M. R. Zou, J. Sayegh, Q. Yan, Epigenetic regulation by lysine demethylase 5 (KDM5) enzymes in cancer. *Cancers* **3**, 1383–1404 (2011).
9. S. V. Sharma, D. Y. Lee, B. Li, M. P. Quinlan, F. Takahashi, S. Maheswaran, U. McDermott, N. Azizian, L. Zou, M. A. Fischbach, K. K. Wong, K. Brandstetter, B. Wittner, S. Ramaswamy, M. Classon, J. Settleman, A chromatin-mediated reversible drug-tolerant state in cancer cell subpopulations. *Cell* **141**, 69–80 (2010).
10. W. Sheng, M. W. LaFleur, T. H. Nguyen, S. Chen, A. Chakravarthy, J. R. Conway, Y. Li, H. Chen, H. Yang, P. H. Hsu, E. M. Van Allen, G. J. Freeman, D. D. De Carvalho, H. H. He, A. H. Sharpe, Y. Shi, LSD1 ablation stimulates anti-tumor immunity and enables checkpoint blockade. *Cell* **174**, 549–563.e19 (2018).
11. D. Peng, I. Kryczek, N. Nagarsheth, L. Zhao, S. Wei, W. Wang, Y. Sun, E. Zhao, L. Vatan, W. Szeliga, J. Kotarski, R. Tarkowski, Y. Dou, K. Cho, S. Hensley-Alford, A. Munkarah, R. Liu, W. Zou, Epigenetic silencing of T_H1-type chemokines shapes tumour immunity and immunotherapy. *Nature* **27**, 249–253 (2015).
12. Y. Qin, S. N. Vasilatos, L. Chen, H. Wu, Z. Cao, Y. Fu, M. Huang, A. M. Vlad, B. Lu, S. Oesterreich, N. E. Davidson, Y. Huang, Inhibition of histone lysine-specific demethylase 1 elicits breast tumor immunity and enhances antitumor efficacy of immune checkpoint blockade. *Oncogene* **38**, 390–405 (2019).
13. R. S. Herbst, J.-C. Soria, M. Kowanetz, G. D. Fine, O. Hamid, M. S. Gordon, J. A. Sosman, D. F. McDermott, J. D. Powderly, S. N. Gettinger, H. E. Kohrt, L. Horn, D. P. Lawrence, S. Rost, M. Leabman, Y. Xiao, A. Mokatrin, H. Koeppen, P. S. Hegde, I. Mellman, D. S. Chen, F. S. Hodi, Predictive correlates of response to the anti-PD-L1 antibody MPDL3280A in cancer patients. *Nature* **515**, 563–567 (2014).
14. J. Nsengimana, J. Laye, A. Filia, S. O'Shea, S. Muralidhar, J. Poźniak, A. Droop, M. Chan, C. Walker, L. Parkinson, J. Gascoyne, T. Mell, M. Polso, R. Jewell, J. Randerson-Moor, G. P. Cook, D. T. Bishop, J. Newton-Bishop, β-Catenin-mediated immune evasion pathway frequently operates in primary cutaneous melanomas. *J. Clin. Invest.* **128**, 2048–2063 (2018).
15. Cancer Genome Atlas Network, Genomic classification of cutaneous melanoma. *Cell* **161**, 1681–1696 (2015).
16. D. Liu, B. Schilling, D. Liu, A. Sucker, E. Livingstone, L. Jerby-Amon, L. Zimmer, R. Gutzmer, I. Satzger, C. Loquai, S. Grabbe, N. Vokes, C. A. Margolis, J. Conway, M. X. He, H. Elmarakeby, F. Dietlein, D. Miao, A. Tracy, H. Gogas, S. M. Goldinger, J. Utikal, C. U. Blank, R. Rauschenberg, D. von Bubnoff, A. Krackhardt, B. Weide, S. Haferkamp, F. Kiecker, B. Izar, L. Garraway, A. Regev, K. Flaherty, A. Paschen, E. M. Van Allen, D. Schadendorf, Integrative molecular and clinical modeling of clinical outcomes to PD1 blockade in patients with metastatic melanoma. *Nat. Med.* **25**, 1916–1927 (2019).
17. N. Riaz, J. J. Havel, V. Makarov, A. Desrichard, W. J. Urba, J. S. Sims, F. S. Hodi, S. Martín-Algarra, R. Mandal, W. H. Sharfman, S. Bhatia, W. J. Hwu, T. F. Gajewski, C. L. Slingluff, D. Chowell, S. M. Kendall, H. Chang, R. Shah, F. Kuo, L. G. T. Morris, J. W. Sidhom, J. P. Schneck, C. E. Horak, N. Weinhold, T. A. Chan, Tumor and microenvironment evolution during immunotherapy with nivolumab. *Cell* **171**, 934–949.e16 (2017).
18. T. H. Hsiao, H. I. Chen, J. Y. Lu, P. Y. Lin, C. Keller, S. Comerford, G. E. Tomlinson, Y. Chen, Utilizing *signature*-score to identify oncogenic pathways of cholangiocarcinoma. *Transl. Cancer Res.* **2**, 6–17 (2013).
19. A. M. Goodman, S. Kato, L. Bazhenova, S. P. Patel, G. M. Frampton, V. Miller, P. J. Stephens, G. A. Daniels, R. Kurzrock, Tumor mutational burden as an independent predictor of response to immunotherapy in diverse cancers. *Mol. Cancer Ther.* **16**, 2598–2608 (2017).
20. M. Ayers, J. Lunceford, M. Nebozhyn, E. Murphy, A. Loboda, D. R. Kaufman, A. Albright, J. D. Cheng, S. P. Kang, V. Shankaran, S. A. Piha-Paul, J. Yearley, T. Y. Seiwert, A. Ribas, T. K. McClanahan, IFN-γ-related mRNA profile predicts clinical response to PD-1 blockade. *J. Clin. Invest.* **127**, 2930–2940 (2017).
21. R. Cristescu, R. Mogg, M. Ayers, A. Albright, E. Murphy, J. Yearley, X. Sher, X. Q. Liu, H. Lu, M. Nebozhyn, C. Zhang, J. K. Lunceford, A. Joe, J. Cheng, A. L. Webber, N. Ibrahim, E. R. Plimack, P. A. Ott, T. Y. Seiwert, A. Ribas, T. K. McClanahan, J. E. Tomassini, A. Loboda, D. Kaufman, Pan-tumor genomic biomarkers for PD-1 checkpoint blockade-based immunotherapy. *Science* **362**, eaar3593 (2018).
22. M. S. Rooney, S. A. Shukla, C. J. Wu, G. Getz, N. Hacohen, Molecular and genetic properties of tumors associated with local immune cytolytic activity. *Cell* **160**, 48–61 (2015).
23. M. A. Curran, W. Montalvo, H. Yagita, J. P. Allison, PD-1 and CTLA-4 combination blockade expands infiltrating T cells and reduces regulatory T and myeloid cells within B16 melanoma tumors. *Proc. Natl. Acad. Sci. U.S.A.* **107**, 4275–4280 (2010).
24. H. Karatas, E. C. Townsend, F. Cao, Y. Chen, D. Bernard, L. Liu, M. Lei, Y. Dou, S. Wang, High-affinity, small-molecule peptidomimetic inhibitors of MLL1/WDR5 protein-protein interaction. *J. Am. Chem. Soc.* **135**, 669–682 (2013).
25. M. Gale, J. Sayegh, J. Cao, M. Norcia, P. Gareiss, D. Hoyer, J. S. Merkel, Q. Yan, Screen-identified selective inhibitor of lysine demethylase 5A blocks cancer cell growth and drug resistance. *Oncotarget* **7**, 39931–39944 (2016).
26. J. Zhang, X. Bu, H. Wang, Y. Zhu, Y. Geng, N. T. Nihira, Y. Tan, Y. Ci, F. Wu, X. Dai, J. Guo, Y. H. Huang, C. Fan, S. Ren, Y. Sun, G. J. Freeman, P. Sicinski, W. Wei, Cyclin D-CDK4 kinase destabilizes PD-L1 via cullin 3-SPOP to control cancer immune surveillance. *Nature* **553**, 91–95 (2018).
27. J. B. A. G. Haanen, Converting cold into hot tumors by combining immunotherapies. *Cell* **170**, 1055–1056 (2017).
28. A. T. Parsa, J. S. Waldron, A. Panner, C. A. Crane, I. F. Parney, J. J. Barry, K. E. Cachola, J. C. Murray, T. Tihan, M. C. Jensen, P. S. Mischel, D. Stokoe, R. O. Pieper, Loss of tumor suppressor PTEN function increases B7-H1 expression and immunoresistance in glioma. *Nat. Med.* **13**, 84–88 (2007).
29. M. L. Beshiri, K. B. Holmes, W. F. Richter, S. Hess, A. B. Islam, Q. Yan, L. Plante, L. Litovchick, N. Gévry, N. Lopez-Bigas, W. G. Kaelin, E. V. Benevolenskaya, Coordinated repression of cell cycle genes by KDM5A and E2F4 during differentiation. *Proc. Natl. Acad. Sci. U.S.A.* **109**, 18499–18504 (2012).
30. K. J. Lastwika, W. Wilson III, Q. K. Li, J. Norris, H. Xu, S. R. Ghazarian, H. Kitagawa, S. Kawabata, J. M. Taube, S. Yao, L. N. Liu, J. J. Gills, P. A. Dennis, Control of PD-L1 expression by oncogenic activation of the AKT-mTOR pathway in non-small cell lung cancer. *Cancer Res.* **76**, 227–238 (2016).
31. E. A. Mittendorf, A. V. Philips, F. Meric-Bernstam, N. Qiao, Y. Wu, S. Harrington, X. Su, Y. Wang, A. M. Gonzalez-Angulo, A. Akcakanat, A. Chawla, M. Curran, P. Hwu, P. Sharma, J. K. Litton, J. J. Molldrem, G. Alatrash, PD-L1 expression in triple-negative breast cancer. *Cancer Immunol. Res.* **2**, 361–370 (2014).
32. Y. Sun, M. Yu, M. Qu, Y. Ma, D. Zheng, Y. Yue, S. Guo, L. Tang, G. Li, W. Zheng, M. Wang, D. Guo, C. Li, Hepatitis B virus-triggered PTEN/β-catenin/c-Myc signaling enhances PD-L1

expression to promote immune evasion. *Am. J. Physiol. Gastrointest. Liver Physiol.* **18**, G162–G173 (2020).
33. W. Shao, S. Li, L. Li, K. Lin, X. Liu, H. Wang, H. Wang, D. Wang, Chemical genomics reveals inhibition of breast cancer lung metastasis by Ponatinib via c-Jun. *Protein Cell* **10**, 161–177 (2019).
34. S. Goel, M. J. DeCristo, A. C. Watt, H. BrinJones, J. Sceneay, B. B. Li, N. Khan, J. M. Ubellacker, S. Xie, O. Metzger-Filho, J. Hoog, M. J. Ellis, C. X. Ma, S. Ramm, I. E. Krop, E. P. Winer, T. M. Roberts, H. J. Kim, S. S. McAllister, J. J. Zhao, CDK4/6 inhibition triggers anti-tumour immunity. *Nature* **548**, 471–475 (2017).
35. Clinical Trials Using Palbociclib supported by National Cancer Institute; www.cancer.gov/about-cancer/treatment/clinical-trials/intervention/palbociclib.
36. H. Kim, V. Khanna, T. A. Kucaba, W. Zhang, D. Sehgal, D. M. Ferguson, D. S. Griffith, J. Panyam, TLR7/8 agonist-loaded nanoparticles augment NK cell-mediated antibody-based cancer immunotherapy. *Mol. Pharm.* **17**, 2109–2124 (2020).
37. S. R. Mullins, J. P. Vasilakos, K. Deschler, I. Grigsby, P. Gillis, J. John, M. J. Elder, J. Swales, E. Timosenko, Z. Cooper, S. J. Dovedi, A. J. Leishman, N. Luheshi, J. Elvecrog, A. Tilahun, R. Goodwin, R. Herbst, M. A. Tomai, R. W. Wilkinson, Intratumoral immunotherapy with TLR7/8 agonist MEDI9197 modulates the tumor microenvironment leading to enhanced activity when combined with other immunotherapies. *J. Immunother. Cancer* **7**, 244 (2019).
38. F. Sato-Kaneko, S. Yao, A. Ahmadi, S. S. Zhang, T. Hosoya, M. M. Kaneda, J. A. Varner, M. Pu, K. S. Messer, C. Guiducci, R. L. Coffman, K. Kitaura, T. Matsutani, R. Suzuki, D. A. Carson, T. Hayashi, E. E. Cohen, Combination immunotherapy with TLR agonists and checkpoint inhibitors suppresses head and neck cancer. *JCI Insight* **2**, e93397 (2017).
39. T. Kawai, S. Akira, TLR signaling. *Cell Death Differ.* **13**, 816–825 (2006).
40. J. Tang, A. Shalabi, V. M. Hubbard-Lucey, Comprehensive analysis of the clinical immuno-oncology landscape. *Ann. Oncol.* **29**, 84–91 (2018).
41. H. Tang, Y. Wang, L. K. Chlewicki, Y. Zhang, J. Guo, W. Liang, J. Wang, X. Wang, Y. X. Fu, Facilitating T cell infiltration in tumor microenvironment overcomes resistance to PD-L1 blockade. *Cancer Cell* **29**, 285–296 (2016).
42. J. A. Trujillo, R. F. Sweis, R. Bao, J. J. Luke, T cell-inflamed versus non-T cell-inflamed tumors: A conceptual framework for cancer immunotherapy drug development and combination therapy selection. *Cancer Immunol. Res.* **6**, 990–1000 (2018).
43. A. Kallies, K. L. Good-Jacobson, Transcription factor T-bet orchestrates lineage development and function in the immune system. *Trends Immunol.* **38**, 287–297 (2017).
44. M. Buggert, J. Tauriainen, T. Yamamoto, J. Frederiksen, M. A. Ivarsson, J. Michaëlsson, O. Lund, B. Hejdeman, M. Jansson, A. Sönnerborg, R. A. Koup, M. R. Betts, A. C. Karlsson, T-bet and eomes are differentially linked to the exhausted phenotype of $CD8^+$ T cells in HIV infection. *PLOS Pathog.* **10**, e1004251 (2014).
45. J. Nikolich-Zugich, M. K. Slifka, I. Messaoudi, The many important facets of T-cell repertoire diversity. *Nat. Rev. Immunol.* **4**, 123–132 (2004).
46. Q. Qi, Y. Liu, Y. Cheng, J. Glanville, D. Zhang, J. Y. Lee, R. A. Olshen, C. M. Weyand, S. D. Boyd, J. J. Goronzy, Diversity and clonal selection in the human T-cell repertoire. *Proc. Natl. Acad. Sci. U.S.A.* **111**, 13139–13144 (2014).
47. W. Scheper, S. Kelderman, L. F. Fanchi, C. Linnemann, G. Bendle, M. A. J. de Rooij, C. Hirt, R. Mezzadra, M. Slagter, K. Dijkstra, R. J. C. Kluin, P. Snaebjornsson, K. Milne, B. H. Nelson, H. Zijlmans, G. Kenter, E. E. Voest, J. B. A. G. Haanen, T. N. Schumacher, Low and variable tumor reactivity of the intratumoral TCR repertoire in human cancers. *Nat. Med.* **25**, 89–94 (2019).
48. D. W. Mullins, S. L. Sheasley, R. M. Ream, T. N. Bullock, Y. X. Fu, V. H. Engelhard, Route of immunization with peptide-pulsed dendritic cells controls the distribution of memory and effector T cells in lymphoid tissues and determines the pattern of regional tumor control. *J. Exp. Med.* **198**, 1023–1034 (2003).
49. C. Berger, M. C. Jensen, P. M. Lansdorp, M. Gough, C. Elliott, S. R. Riddell, Adoptive transfer of effector $CD8^+$ T cells derived from central memory cells establishes persistent T cell memory in primates. *J. Clin. Invest.* **118**, 294–305 (2008).
50. S. Spranger, R. Bao, T. F. Gajewski, Melanoma-intrinsic β-catenin signalling prevents anti-tumour immunity. *Nature* **523**, 231–235 (2015).
51. X. Li, Y. Xiang, F. Li, C. Yin, B. Li, X. Ke, WNT/β-catenin signaling pathway regulating T cell-inflammation in the tumor microenvironment. *Front. Immunol.* **10**, 2293 (2019).
52. M. M. Kaneda, K. S. Messer, N. Ralainirina, H. Li, C. J. Leem, S. Gorjestani, G. Woo, A. V. Nguyen, C. C. Figueiredo, P. Foubert, M. C. Schmid, M. Pink, D. G. Winkler, M. Rausch, V. J. Palombella, J. Kutok, K. McGovern, K. A. Frazer, X. Wu, M. Karin, R. Sasik, E. E. Cohen, J. A. Varner, PI3Kγ is a molecular switch that controls immune suppression. *Nature* **539**, 437–442 (2016).
53. F. Raggi, M. C. Bosco, Targeting mononuclear phagocyte receptors in cancer immunotherapy: New perspectives of the triggering receptor expressed on myeloid cells (TREM-1). *Cancers* **12**, 1337 (2020).
54. R. Brian, M. C. Lisa, Macrophages and therapeutic resistance in cancer. *Cancer Cell* **27**, 462–472 (2015).
55. J. E. Kim, M. A. Patel, A. Mangraviti, E. S. Kim, D. Theodros, E. Velarde, A. Liu, E. W. Sankey, A. Tam, H. Xu, D. Mathios, C. M. Jackson, S. Harris-Bookman, T. Garzon-Muvdi, M. Sheu, A. M. Martin, B. M. Tyler, P. T. Tran, X. Ye, A. Olivi, J. M. Taube, P. C. Burger, C. G. Drake, H. Brem, D. M. Pardoll, M. Lim, Combination therapy with anti-PD-1, anti-TIM-3, and focal radiation results in regression of murine gliomas. *Clin. Cancer Res.* **23**, 124–136 (2017).
56. P. Sharma, S. Hu-Lieskovan, J. A. Wargo, A. Ribas, Primary, adaptive, and acquired resistance to cancer immunotherapy. *Cell* **168**, 707–723 (2017).
57. C. Lu, A. V. Paschall, H. Shi, N. Savage, J. L. Waller, M. E. Sabbatini, N. H. Oberlies, C. Pearce, K. Liu, The MLL1-H3K4me3 axis-mediated PD-L1 expression and pancreatic cancer immune evasion. *J. Natl. Cancer. Inst.* **109**, djw283 (2017).
58. J. M. Taube, R. A. Anders, G. D. Young, H. Xu, R. Sharma, T. L. McMiller, S. Chen, A. P. Klein, D. M. Pardoll, S. L. Topalian, L. Chen, Colocalization of inflammatory response with B7-h1 expression in human melanocytic lesions supports an adaptive resistance mechanism of immune escape. *Sci. Transl. Med.* **4**, 127ra37 (2012).
59. P. C. Tumeh, C. L. Harview, J. H. Yearley, I. P. Shintaku, E. J. Taylor, L. Robert, B. Chmielowski, M. Spasic, G. Henry, V. Ciobanu, A. N. West, M. Carmona, C. Kivork, E. Seja, G. Cherry, A. J. Gutierrez, T. R. Grogan, C. Mateus, G. Tomasic, J. A. Glaspy, R. O. Emerson, H. Robins, R. H. Pierce, D. A. Elashoff, C. Robert, A. Ribas, PD-1 blockade induces responses by inhibiting adaptive immune resistance. *Nature* **515**, 568–571 (2014).
60. H. Tang, Y. Liang, R. A. Anders, J. M. Taube, X. Qiu, A. Mulgaonkar, X. Liu, S. M. Harrington, J. Guo, Y. Xin, Y. Xiong, K. Nham, W. Silvers, G. Hao, X. Sun, M. Chen, R. Hannan, J. Qiao, H. Dong, H. Peng, Y. X. Fu, PD-L1 on host cells is essential for PD-L1 blockade-mediated tumor regression. *J. Clin. Invest.* **128**, 580–588 (2018).
61. H. Lin, S. Wei, E. M. Hurt, M. D. Green, L. Zhao, L. Vatan, W. Szeliga, R. Herbst, P. W. Harms, L. A. Fecher, P. Vats, A. M. Chinnaiyan, C. D. Lao, T. S. Lawrence, M. Wicha, J. Hamanishi, M. Mandai, I. Kryczek, W. Zou, Host expression of PD-L1 determines efficacy of PD-L1 pathway blockade-mediated tumor regression. *J. Clin. Invest.* **128**, 1708 (2018).
62. L. Hijmering-Kappelle, J. Hiltermann, B. Hiddinga, A. van der Wekken, N. Hart, H. Groen, W. Timens, PD-L1 expression, CD8 cells and MHC-class-1 Beta-2-microglobulin expression in advanced non-small lung cancer. Abstract presented at AACR Annual Meeting 2019, Atlanta, GA, March 29–April 3, 2019.
63. S. Wang, Z. He, X. Wang, H. Li, X.-S. Liu, Antigen presentation and tumor immunogenicity in cancer immunotherapy response prediction. *eLife* **8**, e49020 (2019).
64. S. J. Szabo, S. T. Kim, G. L. Costa, X. Zhang, C. G. Fathman, L. H. Glimcher, A novel transcription factor, T-bet, directs Th1 lineage commitment. *Cell* **100**, 655–669 (2000).
65. F. Cruz-Guilloty, M. E. Pipkin, I. M. Djuretic, D. Levanon, J. Lotem, M. G. Lichtenheld, Y. Groner, A. Rao, Runx3 and T-box proteins cooperate to establish the transcriptional program of effector CTLs. *J. Exp. Med.* **206**, 51–59 (2009).
66. A. Sindrilaru, T. Peters, S. Wieschalka, C. Baican, A. Baican, H. Peter, A. Hainzl, S. Schatz, Y. Qi, A. Schlecht, J. M. Weiss, M. Wlaschek, C. Sunderkötter, K. Scharffetter-Kochanek, An unrestrained proinflammatory M1 macrophage population induced by iron impairs wound healing in humans and mice. *J. Clin. Invest.* **121**, 985–997 (2011).
67. C. M. Ohri, A. Shikotra, R. H. Green, D. A. Waller, P. Bradding, Macrophages within NSCLC tumour islets are predominantly of a cytotoxic M1 phenotype associated with extended survival. *Eur. Respir. J.* **33**, 118–126 (2009).
68. N. Lopez-Bigas, T. A. Kisiel, D. C. Dewaal, K. B. Holmes, T. L. Volkert, S. Gupta, J. Love, H. L. Murray, R. A. Young, E. V. Benevolenskaya, Genome-wide analysis of the H3K4 histone demethylase RBP2 reveals a transcriptional program controlling differentiation. *Mol. Cell* **31**, 520–530 (2008).
69. D. Zhao, Q. Zhang, Y. Liu, X. Li, K. Zhao, Y. Ding, Z. Li, Q. Shen, C. Wang, N. Li, X. Cao, H3K4me3 demethylase Kdm5a is required for NK cell activation by associating with p50 to suppress SOCS1. *Cell Rep.* **15**, 288–299 (2016).
70. M. E. Ritchie, B. Phipson, D. Wu, Y. Hu, C. W. Law, W. Shi, G. K. Smyth, *limma* powers differential expression analyses for RNA-sequencing and microarray studies. *Nucleic. Acids. Res.* **43**, e47 (2015).
71. M. I. Love, W. Huber, S. Anders, Moderated estimation of fold change and dispersion for RNA-seq data with DESeq2. *Genome Biol.* **15**, 550 (2014).
72. A. Subramanian, P. Tamayo, V. K. Mootha, S. Mukherjee, B. L. Ebert, M. A. Gillette, A. Paulovich, S. L. Pomeroy, T. R. Golub, E. S. Lander, J. P. Mesirov, Gene set enrichment analysis: A knowledge-based approach for interpreting genome-wide expression profiles. *Proc. Natl. Acad. Sci. U.S.A.* **102**, 15545–15550 (2005).
73. Y. Liao, G. K. Smyth, W. Shi, featureCounts: An efficient general purpose program for assigning sequence reads to genomic features. *Bioinformatics* **30**, 923–930 (2014).
74. F. A. Ran, P. D. Hsu, J. Wright, V. Agarwala, D. A. Scott, F. Zhang, Genome engineering using the CRISPR-Cas9 system. *Nat. Protoc.* **8**, 2281–2308 (2013).
75. D. W. Huang, B. T. Sherman, R. A. Lempicki, Systematic and integrative analysis of large gene lists using DAVID bioinformatics resources. *Nat. Protoc.* **4**, 44–57 (2009).
76. S. Picelli, Å. K. Björklund, O. R. Faridani, S. Sagasser, G. Winberg, R. Sandberg, Smart-seq2 for sensitive full-length transcriptome profiling in single cells. *Nat. Methods* **10**, 1096–1098 (2013).
77. M. Yousfi Monod, V. Giudicelli, D. Chaume, M. P. Lefranc, IMGT/JunctionAnalysis: The first tool for the analysis of the immunoglobulin and T cell receptor complex V-J and V-D-J JUNCTIONs. *Bioinformatics* **20**, i379–i385 (2004).

Acknowledgments: We thank Y. Zhang at Tsinghua University for the gift of the MyD88 knockout mice. We also thank P. Jiao at Center of Biomedical Analysis in Tsinghua University for technical assistance with flow cytometry analysis. Editorial services were provided by N. R. Gough (BioSerendipity LLC, Elkridge, MD). **Funding:** This work was supported by a Chinese National Major Scientific Research Program grant from the Ministry of Science and Technology of the People's Republic of China (no. 2015CB943200 to X.L.), the National Natural Science Foundation of China (NSFC) (no. 21877067 to X.L. and no. 81673460 to D.W.), the China Postdoctoral Science Foundation (2017 M620753 to L.W.), Beijing Advanced Innovation Center for Human Brain Protection (to X.L.), and the Tsinghua-Peking Joint Center for Life Sciences Postdoctoral Foundation (to L.W.). **Author contributions:** X.L., L.W., and Y.G. designed the study. L.W., Y.G., D.L., L.H., Zhenda Wang, Zhisong Wang, J.S., and F.N. performed all experiments. S.G. and R.A. analyzed mouse transcriptomics data. H.D. analyzed proteomics data. J.Z., L.C.H., G.Z., C.C., and Z. Wei performed the transcriptome and exome analysis of the *Kdm5a* gene and *Kdm5a* gene signature from published sources. X.L., L.W., Y.G., L.C.H., G.Z., D.W., X.H., and W.W. contributed to the interpretation of the results and wrote the paper. D.S.D., L.C.H., Y.H., X.H., and Y.S. edited the paper. X.L. supervised the project. **Competing interests:** X.L. holds a patent for D18 (#ZL 2017 1 1146690.1). All other authors declare that they have no competing interests. **Data and materials availability:** All the data are included in the main text or in the Supplementary Materials. Raw RNA-seq data files are deposited in the National Center for Biotechnology Information Gene Expression Omnibus database (GSE146784). D18 is available from X.L. under a material transfer agreement with Tsinghua University.

Submitted 5 March 2019
Resubmitted 22 December 2019
Accepted 23 July 2020
Published 9 September 2020
10.1126/scitranslmed.aax2282

Citation: L. Wang, Y. Gao, G. Zhang, D. Li, Z. Wang, J. Zhang, L. C. Hermida, L. He, Z. Wang, J. Si, S. Geng, R. Ai, F. Ning, C. Cheng, H. Deng, D. S. Dimitrov, Y. Sun, Y. Huang, D. Wang, X. Hu, Z. Wei, W. Wang, X. Liao, Enhancing KDM5A and TLR activity improves the response to immune checkpoint blockade. *Sci. Transl. Med.* **12**, eaax2282 (2020).

Science Translational Medicine

Enhancing KDM5A and TLR activity improves the response to immune checkpoint blockade

Liangliang Wang, Yan Gao, Gao Zhang, Dan Li, Zhenda Wang, Jie Zhang, Leandro C. Hermida, Lei He, Zhisong Wang, Jingwen Si, Shuang Geng, Rizi Ai, Fei Ning, Chaoran Cheng, Haiteng Deng, Dimiter S. Dimitrov, Yan Sun, Yanyi Huang, Dong Wang, Xiaoyu Hu, Zhi Wei, Wei Wang and Xuebin Liao

Sci Transl Med **12**, eaax2282.
DOI: 10.1126/scitranslmed.aax2282

All roads lead to antitumor immunity

Immune checkpoint blockade immunotherapy for cancer has been achieving increasing prominence in recent years, but, unfortunately, it still only works for a subset of patients and tumor types. Wang *et al.* found that higher expression of lysine demethylase KDM5A in tumors correlates with their responses to immune checkpoint inhibition. The authors then found a way to take advantage of this mechanism using a compound that increased both KDM5A and a key immune checkpoint protein. At the same time, this compound also activated Toll-like receptor signaling, further stimulating antitumor immunity in multiple mouse models.